Chapter 2
Size Effects on Semiconductor Nanoparticles

Rolf Koole, Esther Groeneveld, Daniel Vanmaekelbergh, Andries Meijerink and Celso de Mello Donegá

Abstract This chapter addresses the fundamental concepts needed to understand the impact of size reduction on the electronic structure and optoelectronic properties of semiconductor nanostructures, with emphasis on quantum confinement effects. This effect is explained by two different approaches: the "top-down" and the "bottom-up". Subsequently, a brief description of the optical properties of semiconductor nanocrystals is presented. This is followed by sections discussing the essential characteristics of nanocrystals consisting of two (or more) different semiconductors joined together by heterointerfaces (i.e., heteronanocrystals). Moreover, the essential differences between the impact of size reduction on semiconductors in comparison to metals and insulators is discussed. The chapter ends by briefly discussing the potential applications of semiconductor nanoparticles.

2.1 Introduction

There is currently a strong drive among scientists to explore the possibilities of making and characterizing materials of ever smaller dimensions. This effort is motivated by two factors. First of all, there is a great fundamental interest in the novel properties that arise when the dimensions of a material reach the nanoscale (see Chap. 1). Besides the fundamental interest, the wide range of potential applications based on nanomaterials provides an important driving force to push the size of materials to the smallest limits. The most illustrative example is that of the chip-technology, where the continuation of Moore's law has dictated industry to make ever smaller transistors, which recently became only a few tens of nanometers wide [1]. As another example, the large effective surface area that can be achieved using nanomaterials can be very beneficial in catalytic applications. Moreover, the tunable properties of nanomaterials are very attractive for a variety of technologies,

R. Koole · E. Groeneveld · D. Vanmaekelbergh · A. Meijerink · C. de Mello Donegá (✉)
Debye Institute for Nanomaterials Science, Utrecht University, Utrecht, The Netherlands
e-mail: c.demello-donega@uu.nl

C. de Mello Donegá (ed.), *Nanoparticles*,
DOI 10.1007/978-3-662-44823-6_2

Fig. 2.1 Luminescence from suspensions of colloidal CdSe nanocrystals (1.7–4.5 nm diameter, from *left* to *right*) under UV excitation (*courtesy* A. Brinkman and M. Vis, Utrecht University)

ranging from lighting and optoelectronics to biomedical imaging, photovoltaics and thermoelectrics [2].

As discussed in Chap. 1, the impact of spatial confinement is not the same for different materials and/or different properties, as it depends on characteristic length scales of a given property, which are ultimately determined by the material's composition and structure. The profound impact of spatial confinement on the optical properties of semiconductor nanostructures is illustrated in Fig. 2.1. The relevant length scale in this case is the so-calledexciton Bohr radius (a_0), a dimension describing the spatial extension of excitons (i.e., electron-hole pairs) in semiconductors, which ranges from $\sim$2 to $\sim$50 nm depending on the material [3]. The spatial confinement of excitons in semiconductor nanostructures leads to a phenomenon known as quantum confinement [4]. Understanding the origin of quantum confinement and how it influences the electronic structure of semiconductor nanostructures is an essential aspect of Nanoscience. This has stimulated a vast research effort to unravel the fundamental properties of semiconductor nanostructures, leading to great advances in the last few decades [2–9].

This chapter addresses the impact of size reduction on the properties of semiconductor nanostructures, with emphasis on quantum confinement effects. To understand the unique properties that result from quantum confinement, it is instructive to first look at the electronic structure and electronic transitions of bulk semiconductors. Next, the impact of size reduction to the nanoscale on the electronic structure of semiconductors is addressed. Subsequently, a brief description of the optical properties of semiconductor nanocrystals (NCs) is presented. This is followed by sections discussing the essential characteristics of NCs consisting of two (or more) different semiconductors joined together by heterointerfaces. Section 2.8 discusses the essential differences between the impact of size reduction on semiconductors in comparison to metals and insulators. The final section deals with the applications of semiconductor NCs.

2.2 Electronic Structure of Bulk Semiconductors

In contrast to a free electron traveling through vacuum, electrons in a semiconductor experience a periodic potential caused by the atoms in the crystal lattice. To simplify the problem we will start with the description of a hypothetical one dimensional crystal [5], which can be described by the following Hamiltonian:

$$H = H^0 + V(x) = -\frac{\hbar^2}{2m}\frac{\partial^2}{\partial x^2} + V(x) \tag{2.1}$$

where H^0 is the kinetic energy operator, and $V(x)$ describes the periodic potential set by the crystal lattice. The potential is periodic over the lattice constant a, so that $V(x) = V(x + a)$. This means that the Schrödinger equation after translation of the wave function $\psi(x)$ by a distance $a(\psi(x + a))$, can be written as:

$$-\frac{\hbar^2}{2m}\frac{\partial^2}{\partial x^2}\psi(x+a) + V(x)\psi(x+a) = E\psi(x+a) \tag{2.2}$$

After translation over distance a, the wave functions should still have the same eigenvalue E. This implies that the wave functions $\psi(x)$ and $\psi(x + a)$ should only differ by a phase-factor. A wave function that obeys this criterion and that is an eigenfunction of Eq. 2.2 can be written as follows:

$$\psi_{bloch,k}(x) = e^{ikx} \cdot u_k(x) \tag{2.3}$$

where k is defined as the wave vector ($k = 2\pi/\lambda$) and $u_k(x)$ is a function that is periodic with the lattice constant ($u_k(x) = u_k(x + a)$). The resulting wave function is called a Bloch function and is a plane wave (e^{ikx}) that is modulated by a periodic function ($u_k(x)$) [5]. Physically, the plane wave represents the phase (i.e., the sign of the amplitude) of the wave function, whereas $u_k(x)$ describes the response of the valence electrons to the periodic potential of the crystal lattice. Translation of the Bloch function over a distance a gives:

$$\psi_{bloch,k}(x + a) = e^{ika} \cdot \psi_{bloch,k}(x) \tag{2.4}$$

which shows that the wave function indeed only differs by a (phase) constant after translation over a.

Before examining the energy levels of an electron perturbed by the periodic potential of the crystal lattice, we first consider a free electron in vacuum, which is described only by the plane wave $\psi(x) = e^{ikx}$ [5], and has a continuum of energy levels given by the dispersion relation (Fig. 2.2a):

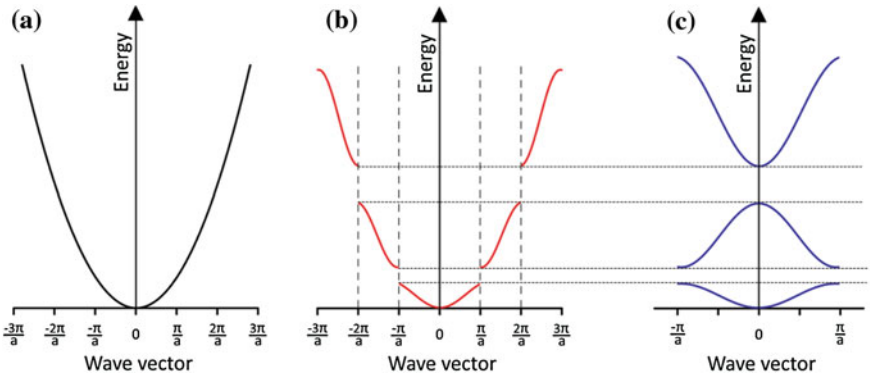

Fig. 2.2 **a** Dispersion relation of a free electron in vacuum. **b** Dispersion relation of an electron in a one dimensional crystal with lattice constant a. **c** Reduced zone representation of the dispersion relation presented in **b**. Reprinted with permission from Ref. [45]

$$E(k) = \frac{\hbar^2 k^2}{2m_0} \tag{2.5}$$

where m_0 is the free electron mass.

The periodic potential in a crystal lattice causes an important change in the dispersion relation for electrons. Electrons that propagate through the lattice with a wavelength that is very different from the lattice spacing a are only slightly disturbed and therefore the energy is similar to that of free electrons. However, when the wavelength of electrons is similar to twice the lattice spacing, or in other words when $k = \pi/a$, the electrons are reflected by the periodic potential of the crystal lattice. These Bragg reflections result in standing waves, described by a linear combination of the plane waves with $k = \pi/a$ and $k = -\pi/a$. The two resulting standing waves ψ^{+}_{bloch} and ψ^{-}_{bloch} are identical, except for a displacement along x by $a/2$. This causes a significant difference in energy between the two standing waves, because the first one concentrates the electron probability at the ions (lowering the potential energy), whereas the second standing wave concentrates the probability exactly in between the ions (increasing the potential energy). Hence, due to the difference in electronic charge distribution, the two standing waves have a different energy at the same k-value, leading to an energy gap in the dispersion relation. The periodicity of the lattice causes Bragg reflections to occur at multiple k-values ($k = n\pi/a$, where n is an integer). This leads to a dispersion relation containing multiple energy gaps, which are referred to as band gaps (Fig. 2.2b).

Another property of the Bloch function is the periodicity in k: wave functions with k-values that differ by $n2\pi/a$ are equivalent, as can be derived from Eq. 2.4. This may be interpreted as follows: the value of the phase (i.e. e^{ikx}) at the ions ($x = qa$, where q is an integer) is exactly the same for k and $k + 2\pi/a$, thus describing the same physical situation. Consequently, the energy dispersion relation may be restricted to k-values between $-\pi/a < k < \pi/a$. Values of larger k can be

folded inside this region by subtracting $2\pi/a$ from the k-value. The resulting interval (in 1 dimension) is called the first Brillouin zone, and the energy dispersion relation can be plotted within this reduced zone (Fig. 2.2c). By reducing the dispersion relation to the interval $-\pi/a < k < \pi/a$, energy bands appear, and one k-value has multiple corresponding energies (which may be regarded as overtones). The band gaps between the different bands occur at $k = \pi/a$ and $k = 0$.

What happens if we consider a semiconductor crystal of more than one dimension? The electronic structure of a three-dimensional (3-D) semiconductor crystal can be explained along the same lines as the 1-D case. However, Bragg reflections in a 3-d crystal lattice are more complex because the periodicity is not the same in different directions. For a simple (primitive) cubic lattice, this means that in the $\langle 110 \rangle$ direction reflection will occur when $k = \sqrt{2}\pi/a$, and in the $\langle 111 \rangle$ direction when $k = \sqrt{3}\pi/a$. This implies that band gaps will arise not only at $k = \pi/a$, but also at $k = \sqrt{2}\pi/a$ (where $k_x = k_y = \pi/a$ and $k_z = 0$) and at $k = \sqrt{3}\pi/a$ (with $k_x = k_y = k_z = \pi/a$). The first Brillouin zone of a simple cubic lattice in 3 dimensions is a plain cube in reciprocal space, and has different band gaps at different points in this Brillouin zone. For the hexagonal close-packed lattice (HCP, e.g., the wurtzite crystal structure of CdSe), the first Brillouin zone is more complicated, as depicted in Fig. 2.3a. The (Greek) letters are the conventional symbols to denote the different points in the Brillouin zone (BZ) of the HCP lattice. For example, the Γ-point is located at $k_{x,y,z} = 0$. It can be seen that there is only one Γ-point in the first BZ of a HCP lattice. In case of a cubic FCC crystal structure (e.g., the rock salt lattice of PbSe, or the zinc blende lattice of CdTe), the first Brillouin Zone has the shape of a truncated octahedron (Fig. 2.3b).

It is difficult to draw the complete dispersion relation as displayed in Fig. 2.2 for a three-dimensional system. The usual way of plotting the energy dependence of electrons in a 3-d semiconductor crystal is shown in Fig. 2.4, which shows the band structure of PbSe as a representative example. The symbols on the x-axis correspond to the symbols in Fig. 2.3b, and the diagram shows the evolution of energy when

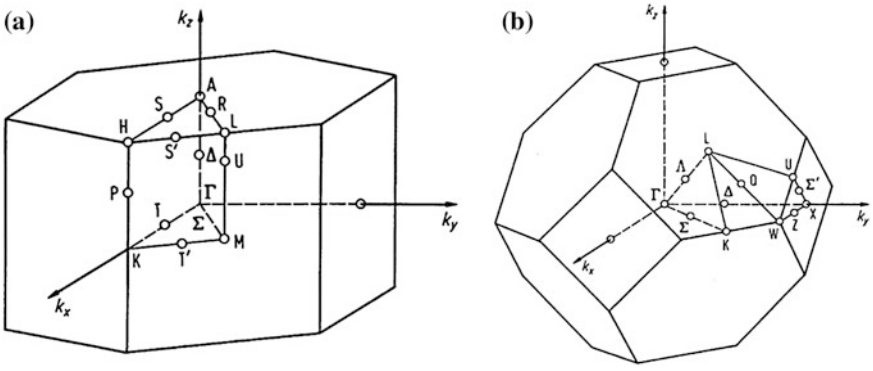

Fig. 2.3 First Brillouin Zone of HCP **a**, and FCC **b** crystal structures. Reprinted with permission from Ref. [19]

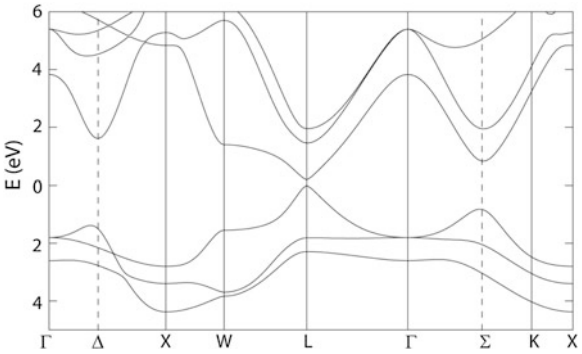

Fig. 2.4 Band structure of bulk PbSe. The zero of energy is at the *top* of the valence band at the L-point, where the fundamental band gap is located. Reprinted with permission from Ref. [46], copyright (2008) Wiley-VCH Verlag GmbH & Co. KGaA, Weinheim

going from one point in the BZ to the other. The highest occupied energy band is called the valence band (VB) and the lowest unoccupied energy band is referred to as conduction band (CB). The energy difference between the VB and CB is referred to as the fundamental band gap. For semiconductors the fundamental energy gap is smaller than 4 eV, which allows electrons to be thermally excited from the VB to the CB at sufficiently high temperatures. The top of the VB and the bottom of the CB for the smallest energy gap can be located at the same *k*-value, yielding a direct band-gap semiconductor (e.g., CdSe), or at different *k*-values, in which case the material is referred to as an indirect band gap semiconductor (e.g., silicon) [5].

It should be noted that band diagrams do *not* show all *k*-values and therefore are only a representation of the dispersion relation for some of the most relevant points in the BZ, in only a few directions in reciprocal space. For example, it is clear from the band structure of PbSe in Fig. 2.4 that the fundamental band gap is located at the L-point in the BZ. In contrast, the fundamental band gap of semiconductors with HCP crystal structure (e.g., wurtzite CdSe) is located at the Γ-point. It is apparent from Fig. 2.3b that there are 8 L-points at the edges of the first BZ of a FCC crystal. Since every L-point is shared by a neighbouring BZ, the fundamental band gap of PbSe is 4-fold degenerate (8-fold including spin). The L-point is in the $\langle 111 \rangle$ direction in reciprocal space, and the four L-states can be seen as states with the same absolute value of *k*, but with a momentum in four different directions ($\langle 111 \rangle$, $\langle 11\text{-}1 \rangle$, $\langle 1\text{-}11 \rangle$, and $\langle \text{-}111 \rangle$).

2.3 Electronic Transitions in Bulk Semiconductors

The valence band (VB) of a semiconductor is completely occupied, while the conduction band (CB) is unoccupied. An electron can be promoted from the VB to the CB as result of an external perturbation, e.g., the absorption of a photon with

energy equal to or higher than the fundamental band gap. The promotion of an electron from the VB to the CB can be described as a system in which the CB contains one particle whereas the VB, consisting of many particles, lacks a particle. This situation is a many-body system. A standard approach to simplify a many-body system is by describing a large number of interacting particles by as little as possible non-interacting particles called '*quasi-particles*' [5]. A first step is the introduction of a *quasi*-particle in the VB, namely 'hole', which is correlated to the ensemble of electrons in the VB from which the electron is removed. The electron in the CB is described by charge (e^-), spin (s = 1/2), and effective mass (m_e^*), whereas the hole in the VB is characterized by a positive charge (e^+), spin (s = 1/2), and effective mass (m_h^*). Due to their charge, electrons and holes are referred to as charge carriers. The concept of effective mass is introduced to account for the interaction of the particle with the periodic crystal lattice. The effective mass thus reflects the increased or decreased mobility of a charge carrier (electron or hole) in the semiconductor with respect to that of an electron in vacuum. An effective mass that is larger than the free electron mass corresponds to an interaction with the crystal lattice that slows down the charge carrier, whereas a higher carrier mobility is reflected in a smaller effective mass. Alternatively, one can take the effective masses as indicators for the spatial extension of the carrier wave function, since the degree of delocalization is inversely proportional to the effective mass of the charge carrier (i.e., lighter carriers are more delocalized).

Since electrons and holes have opposite charges they interact via a Coulomb potential, forming an electron-hole pair that can be described as a *quasi-particle* (the 'exciton'). The formation of an exciton requires a minimum amount of energy given by [5, 10]:

$$E = \hbar\omega = E_g + E_{e,kin} + E_{h,kin} \tag{2.6}$$

in which $E_{e,kin}$ and $E_{h,kin}$ are the kinetic energies of the electron and hole, respectively, and E_g is the semiconductor fundamental band gap. Further, momentum conservation requires that:

$$\hbar k_{cb} = \hbar k_{vb} + \hbar k_{photon} \tag{2.7}$$

where k_{cb} and k_{vb} are the wave vectors of the promoted electron in the CB and the hole in the VB, respectively. Because photons have negligible momentum, the condition $k_{\mathrm{cb}} = k_{\mathrm{vb}}$ must be met. Therefore, without other external perturbations, only transitions within the same k-values (i.e., vertical or direct transitions) can occur [5, 10], as shown in Fig. 2.5.

The energy of an exciton can be expressed by the following dispersion relation:

$$E_n = E_g - \frac{Ry^*}{n^2} + \frac{\hbar^2 k^2}{2(m_e{}^* + m_h{}^*)} \tag{2.8}$$

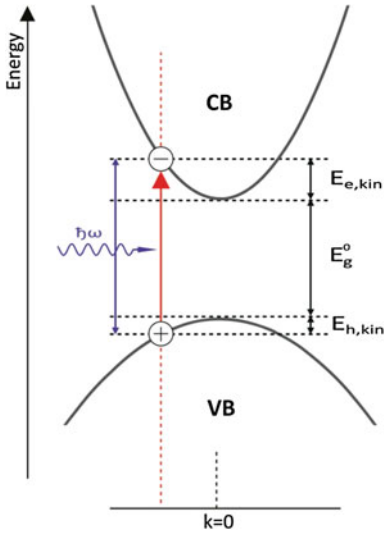

Fig. 2.5 Schematic representation of the promotion of an electron from the valence band to the conduction band in a direct band gap semiconductor as result of the absorption of a photon [5, 10]. Reprinted with permission from Ref. [45]

where the second term contains Hydrogen-like set of energy levels in which Ry^* is the exciton Rydberg energy (corresponds to the ionization energy of the lowest hydrogenic state) [5]. The third term in Eq. 2.8 accounts for the kinetic energy of the exciton centre of mass motion in which k is the exciton wave vector. The kinetic energy term resembles the dispersion curve of a free electron, but with the difference that it is corrected for the effective mass of the exciton. The third term originates from the fact that the interacting holes and electrons can be described as two particles interacting via a Coulomb potential. A Hamiltonian analogous to the hydrogen atom Hamiltonian is used to calculate the energy of the exciton, in which the exciton effective mass replaces the free electron mass m_0. By analogy to the Hydrogen atom the most probable distance between the electron and hole in an exciton is given by the so-called exciton Bohr radius (a_0) [5]

$$a_0 = \frac{\hbar^2 \varepsilon}{e^2}\left(\frac{1}{m_e{}^*} + \frac{1}{m_h{}^*}\right) \tag{2.9}$$

where $m_e{}^*$ and m_h^* are the effective masses of electron and hole, respectively. Further, e is the electron charge and ε is the dielectric constant of the semiconductor. The exciton Bohr radius provides a very useful length scale to describe the spatial extension of excitons in semiconductors, and ranges from $\sim$2 to $\sim$50 nm depending on the semiconductor [3, 5]. It is interesting to note that the exciton Bohr radius a_0 and the band gap of the semiconductor are correlated, so that materials with wider band gaps possess smaller a_0 (e.g., E_g and a_0 are, respectively, 0.26 eV and 46 nm for PbSe, 1.75 eV and 4.9 nm for CdSe, and 3.7 eV and 1.5 nm for ZnS).

2.4 Electronic Structure of Semiconductor Nanocrystals

The description of the band structure of semiconductors presented above was based on an infinite crystal. What happens if the dimensions of the semiconductor crystal are decreased to the nanoscale? As Fig. 2.1 clearly demonstrates, the electronic structure of semiconductor NCs is strongly size dependent. This effect, known as quantum confinement, can be understood via two different approaches. In the first approach ("top-down"), the NC is treated as a small piece of semiconductor material in which the exciton is spatially confined. The second method ("bottom-up") involves a quantum chemical (molecular) approach, in which the NC is build up atom by atom and is treated as an increasingly larger molecular cluster that eventually evolves into a bulk semiconductor crystal. These two approaches will be discussed in the following subsections.

2.4.1 The Top-Down Approach: Nanocrystal as a Small Crystal

In the top-down approach, the Bloch wave functions describing the bulk properties of the semiconductor (including Brillouin zone and band the structure) are maintained, but multiplied by an envelope function to correct for the spatial confinement of the charge carriers (electrons and holes) and the exciton in the small NC [4, 5]:

$$\Psi_{total}(x) = \psi_{bloch}(x) \cdot \varphi_{env}(x) \tag{2.10}$$

The total wave function (Ψ_{tot}) is thus the product of the Bloch function describing the bulk properties of the semiconductor, and the envelope function (φ_{env}) that describes the confinement effects of the charge carriers in the NC. The envelope function is then the solution of the Schrödinger equation for a "particle-in-a-box" problem. For a 3-dimensional box with dimensions L, the wave function would simply be the product of sinusoidal functions in x, y, and z-directions. However, if the confinement is the same in all directions, the NC can better be represented as a spherical potential box (i.e., a quantum dot, QD). The *eigen* functions can then best be described as the product of spherical harmonics ($Y((\theta,\varphi))$) and a radial Bessel function ($R(r)$) [4, 5]:

$$\varphi_{env}(\theta, \phi, r) = Y_l^m(\theta, \phi) \cdot R(r) \tag{2.11}$$

The envelope function has a close resemblance with the wave functions describing the electron of a hydrogen atom. In that case, however, the potential experienced by the electron is determined by the positively charged proton (i.e., V (r) $\sim$ 1/r), while there is no positively charged core in a QD, but instead the electrons experience a spherical potential well of diameter D for which V(r) equals

$-V_0$ (finite) for r < D/2 and zero elsewhere. Inserting Eq. 2.11 in the Schrödinger equation gives the solutions for the discrete energy-levels of a confined electron in a sphere [4, 5]:

$$E_{n,l}^{conf}(D) = \frac{2\hbar^2 \chi_{nl}^2}{m^* D^2} \tag{2.12}$$

where m^* is the effective mass of electrons (or holes), and χ_{nl} are the roots of the Bessel function, which are absolute values depending on (and increasing with) the principal quantum numbers n (1, 2, 3,…) and azimuthal quantum number l (0, 1, 2, 3…, corresponding to s, p, d,…, orbitals) (Fig. 2.6). The lowest energy level ($n = 1$, $l = 0$) has the symmetry of a 1 s orbital in a hydrogen atom (i.e., it is a 1S level). A direct consequence of the difference in the potential function ($V(r)$) between the hydrogen atom and a quantum dot is that the latter system has no restriction of quantum number l with respect to quantum number n, as is the case in the hydrogen atom ($l \leq n - 1$). Therefore the second energy level in a quantum dot has quantum

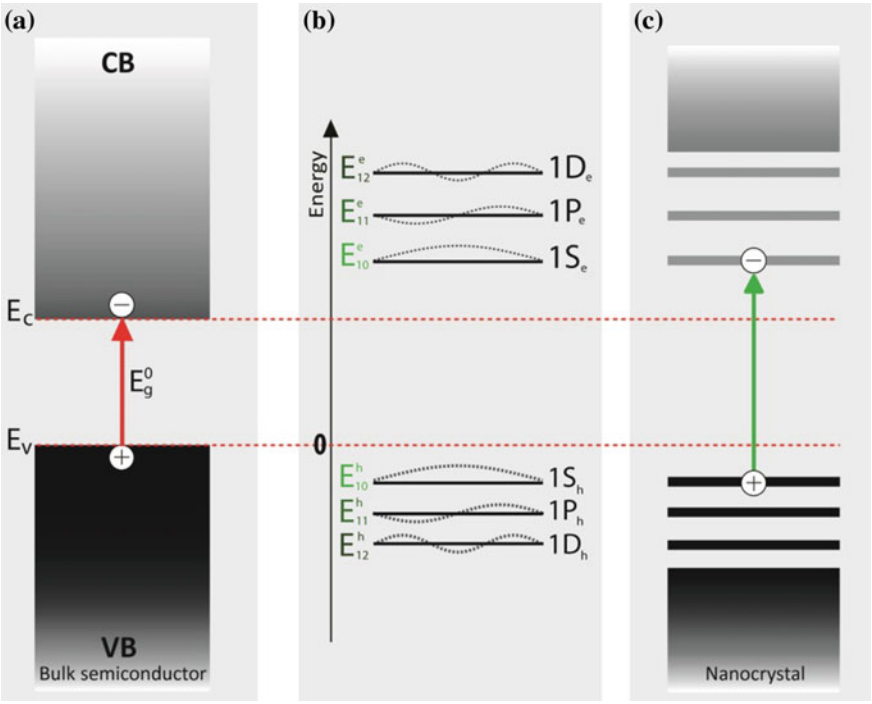

Fig. 2.6 Schematic of the effect of quantum confinement on the electronic structure of a semiconductor. The arrows indicate the lowest energy absorption transition. **a** Bulk semiconductor (CB = conduction band; VB = valence band). **b** Three lowest electron (E_{nl}^e) and hole (E_{nl}^h) energy levels in a quantum dot. The corresponding wave functions are represented by *dashed lines*. **c** Semiconductor nanocrystal (quantum dot). Reprinted with permission from [45]

numbers $n = 1$ and $l = 1$ (i.e., 1P level). The third level is described by $n = 1$, $l = 2$ (1D level), and the fourth level is a 2S level ($n = 2$, $l = 0$). Due to the atomic-like envelope wave functions of the lowest lying energy levels, QDs are often referred to as "artificial atoms".

The band gap of a QD is then the sum of the fundamental bulk band gap (E_g^0) and the confinement energy (E^{conf}) of both electrons and holes:

$$E_g^{tot}(D) = E_g^0 + E_{n,l}^{conf}(D) = E_g^0 + \frac{2\hbar^2\chi_{nl}^2}{m_e^* D^2} + \frac{2\hbar^2\chi_{nl}^2}{m_h^* D^2} \tag{2.13}$$

It should be noted that the electron and hole energy levels are treated independently in the approach above, implying the assumption that the Coulomb interaction between electron and hole is no longer sufficiently strong to form a bound exciton. This approximation is valid only in the so-called strong confinement regime, which holds for NC radius r smaller than the exciton Bohr radius a_0 [4–7]. In this regime the confinement potential becomes larger than the Coulomb interaction. It should be pointed out that the Coulomb interaction is actually much larger than in a bulk crystal, since the charge carriers are confined together in a much smaller volume. However, when $r \ll a_0$ the kinetic energies of the charge carriers are still much larger than the Coulomb interaction between them. Therefore, the electron and hole are no longer correlated and can be treated independently. In first approximation only the change in kinetic energy of the electron and hole are considered, and the Coulomb interaction can be neglected and added later as first order energy corrections.

If the NC radius r is larger than a_0 (viz., weak confinement regime) the increase in exciton energy is due to quantization of the exciton center-of-mass motion [4–7]. The exciton is then described as a particle in a spherical potential, and its discrete energy levels will be given by an expression similar to Eq. (2.12) by replacing the electron (or hole) effective mass by the exciton effective mass. The shift of the energy levels in the weak confinement regime (viz., <100 meV) is much smaller than that in the strong confinement regime. The impact of quantum confinement is usually no longer observable for sizes larger than 2–3 times the exciton Bohr radius.

If the Coulomb interaction is also taken into account the band gap of a QD of radius r can be described as [4–7]

$$E_g(r) = E_g^0 + \frac{\hbar^2\pi^2}{2r^2}\left[\frac{1}{m_e^*} + \frac{1}{m_h^*}\right] - J_{e-h} + E_e^{pol} + E_h^{pol} - 0.248E_{Ry}^* \tag{2.14}$$

where J_{e-h} represents the effective Coulomb interaction between the electron and the hole, which is equal to $1.786e^2/\varepsilon_1 r$ (ε_1 is the dielectric constant of the QD). The terms E_e^{pol} and E_h^{pol} give the self-polarization energies of the electron and hole, respectively, which depend on e^2/r and on the dielectric constants of the QD and the surrounding medium (ε_1 and ε_m, respectively). The exciton Rydberg energy, which accounts for spatial correlation between the electron and the hole, is represented by E_{Ry}^*.

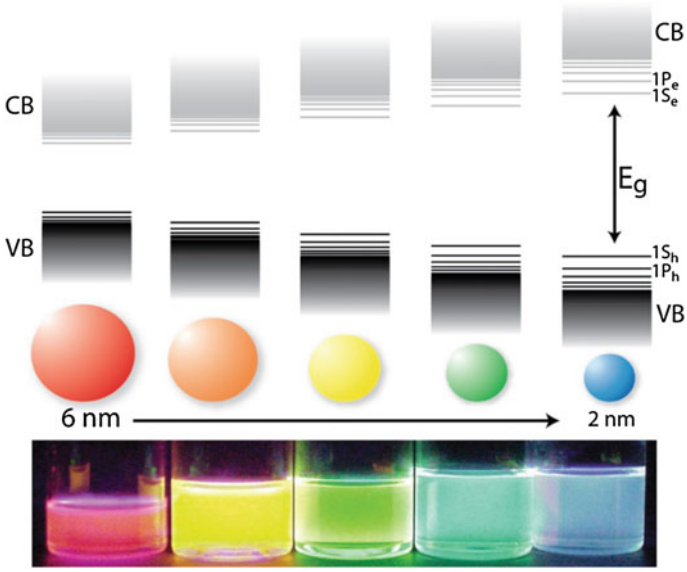

Fig. 2.7 Schematic representation of the quantum confinement effects: the bandgap of the semiconductor material increases with decreasing size, and discrete energy levels arise at the band-edges. Note that the energy difference between the band-edge levels also increases with decreasing size. *Lower panel* shows a photograph of the fluorescence of 5 dispersions of CdSe QDs with different sizes, under excitation with a UV-lamp in the dark. Reproduced by permission of the Royal Society of Chemistry from Ref. [2]

Equations 2.13 and 2.14 clearly describe the two most important consequences of quantum confinement. The first consequence is that the band gap of a semiconductor NC becomes larger with decreasing size, scaling as D^{-2} if the Coulomb interaction is negligible. The second consequence is that discrete energy levels (with different quantum numbers) arise at the band-edges of both the conduction band and valence band. These two size-dependent effects are schematically depicted in Fig. 2.7. In practice, this means that the optical band gap of QDs can be tuned by simply changing their size. For QDs emitting in the visible (e.g.,CdTe or CdSe QDs) this is nicely visualized by their size-dependent luminescence colours (Figs. 2.7 and 2.8).

Quantum confinement effects are also reflected in the optical absorption spectra of QDs. This is illustrated in Fig. 2.8, which shows the absorption spectra of CdTe QDs of different sizes. In the strong quantum confinement regime the energy-spacing between the discrete levels of the envelope functions with different quantum numbers (Eq. 2.12) is in the order of hundreds of meV, and therefore optical transitions between these levels can be clearly resolved in the optical absorption spectrum. Figure 2.8 clearly illustrates that all absorption transitions shift to higher energy as the QD size decreases. The lowest energy optical transition can be assigned to the $1S_h$ to $1S_e$-level (*h* denotes the hole and *e* the electron), the second

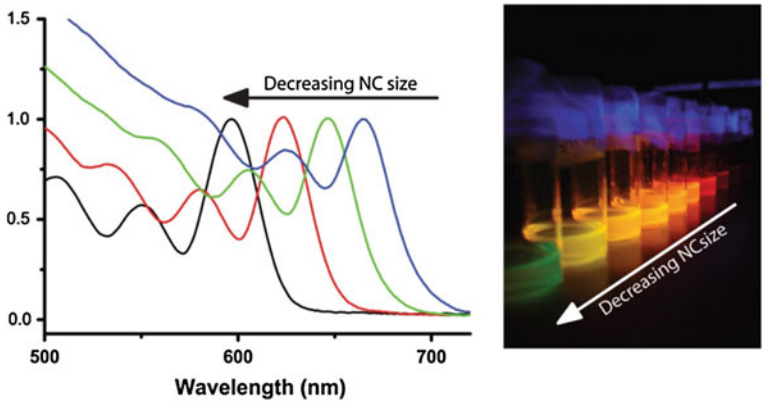

Fig. 2.8 (*Left*) Absorption spectra of colloidal suspensions of CdTe nanocrystal (NC) quantum dots of different sizes. (*Right*) Photograph of vials containing colloidal suspensions of CdTe QDs of different sizes under UV excitation. Reprinted with permission from Ref. [45]

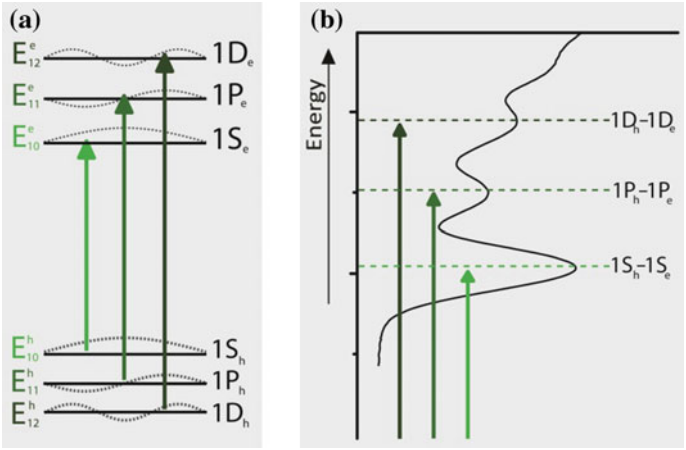

Fig. 2.9 **a** Three lowest electron (E^e_{nl}) and hole (E^h_{nl}) energy levels in a semiconductor nanocrystal quantum dot. The corresponding wavefunctions are represented by the *dashed lines*. Allowed optical transitions are given by the *arrows*. **b** Assignment of the transitions in the absorption spectrum of colloidal CdTe quantum dots. Reprinted with permission from [45]

transition to the $1P_h$ to $1P_e$ level, and so on (Fig. 2.9). The optical selection rules in a QD will be discussed in more detail in Sect. 2.5.

It is interesting to note that the exciton Bohr radius a_0 provides a very convenient length scale to evaluate the impact of quantum confinement on the properties of semiconductor NCs. As discussed above, confinement begins to affect the exciton wave function as the size of the NC approaches a_0. This means that the onset of quantum confinement effects will occur at different NC dimensions for different

semiconductors, since the exciton Bohr radius a_0 varies widely within the semiconductor materials. It is worth noting that a_0 and the band gap E_g are correlated, so that materials with narrower E_g have larger a_0 (e.g., E_g and a_0 are, respectively, 0.26 eV and 46 nm for PbSe, 1.75 eV and 4.9 nm for CdSe, and 3.7 eV and 1.5 nm for ZnS), and will thus experience quantum confinement at larger NC sizes. In contrast, insulators (i.e., materials with $E_g > 4$ eV, e.g., SiO_2, $E_g = 7$ eV) are characterized by strongly localized excitons and hence very small a_0 (typically <1 nm), and are thus affected by quantum confinement only for sizes already in the cluster regime (<20 atoms) [2].

2.4.1.1 Types of Quantum Dots

As discussed above, a semiconductor nanostructure in which the exciton is confined in all three dimensions can be described as a quantum dot, i.e., a structure in which the exciton has no degrees of spatial freedom (zero-dimensional). These so-called quantum confinement effects result in discrete energy levels and larger energy gaps with decreasing sizes. The confinement of electrons and holes in QDs results from the fact that their potential energy is smaller inside the QD than in the surrounding matrix. Such a potential well for charge carriers can be achieved by various architectures, of which three examples are given below (Fig. 2.10).

The first type of QDs is represented by colloidal semiconductor NCs. Colloidal QDs are prepared by wet chemical synthesis, which allow accurate control over the size and shape of the NCs by varying the reaction conditions (see Chap. 6 for details). The potential well for electrons (holes) within the QD is caused by the much higher potential energy of the surrounding medium, which is typically a solvent. The passivating organic ligands that are attached to the surface of the QD

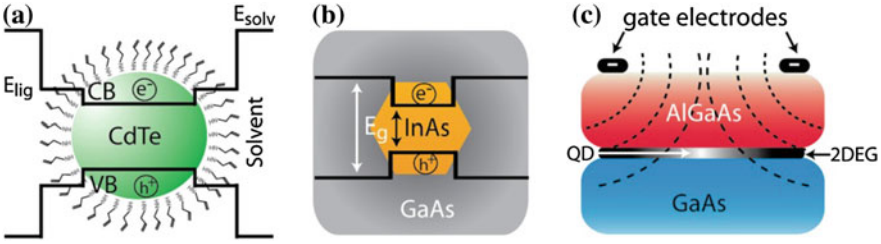

Fig. 2.10 Schematic representation of three types of QD-structures. **a** Colloidal CdTe QD in dispersion. The potential well in the QD is formed by the much higher potential energy for electrons (*holes*) of the surrounding solvent. The organic ligands at the surface of the QD form an intermediate energy barrier. **b** Epitaxially grown InAs QD in a GaAs matrix that has a larger band gap, resulting in a potential well for charge carriers within the InAs QD. **c** Laterally gated QD. A 2-dimensional electron gas (2DEG) is formed at the interface between (n-type) AlGaAs and GaAs and confined in two more dimensions by an electric field generated by gate electrodes on *top* of the device. Reprinted with permission from Ref. [19]

form an intermediate energy barrier between the semiconductor NC and the surrounding medium, as schematically depicted in Fig. 2.10a.

The second example is that of embedded QDs grown by vapour phase epitaxy. These QDs are also known as epitaxial or self-assembled QDs. In this case the potential well for electrons and holes within the semiconductor QD is produced by a surrounding semiconductor material which has a higher conduction band potential and a lower valence band potential (Fig. 2.10b). A typical example of such a system is the combination of small InAs islands embedded in a matrix of GaAs. These structures can be grown with a high degree of control using molecular beam epitaxy (MBE) [11].

The final example concerns a more complicated QD design and is formed in a semiconductor crystal by the field effect of a gate electrode. In such a gated semiconductor QD, one starts with a 2-dimensional electron gas (2DEG) that is formed at the interface between a GaAs and (n-doped) AlGaAs layer. The 2DEG is confined in two more dimensions by applying a negative potential to metal gate electrodes that are deposited on top of the device (Fig. 2.10c). The negative potential causes a depletion of electrons in the 2DEG in the close vicinity of the gate electrodes, which confines the electron to a well-defined spot in between the electrodes. This potential well forms the laterally gated QD [12]. It should be noted that from a fabrication viewpoint this type of QD can also be categorized as epitaxial, since the semiconductor active layers are also deposited by vapour phase epitaxy.

2.4.1.2 Shape Effects

In the discussion above we considered only the case of a spherical quantum dot, in which the exciton is confined in a zero-dimensional spherical potential well. Nevertheless, semiconductor nanostructures can be made with a wide variety of shapes. This is particularly true for colloidal NCs, which can be controllably obtained with a plethora of 0-d (e.g., spheres, cubes, stars, pyramids, and other polyhedra), 1-d (e.g., nanorods, straight or zig-zag wires), and 2-d (e.g., platelets and disks) shapes, as well as with more complex morphologies (e.g., multipods and nanorings) [2] (see Chap. 6 for details). Moreover, vapour phase epitaxial techniques, such as MBE, typically yield non-spherical 0-d (e.g., pyramids) or thin films [11], while a number of techniques is available to grow nanowires [13–15].

It is thus possible to have non-spherical QDs, provided all dimensions are small enough with respect to a_0. In such a case, the electronic structure of the QD will still be characterized by a series of discrete energy levels (Fig. 2.11). The degree of quantum confinement may also vary along different directions depending on the nanostructure shape [3]. If only the diameter of an anisotropic NC is sufficiently small to induce quantum confinement, the exciton will experience a 2-dimensional confinement and the nanocrystal will then be referred to as a Quantum Wire or Quantum Rod, depending on its relative aspect ratio (wires are significantly longer than a_0, while rods have lengths smaller than a few a_0). If the exciton is confined

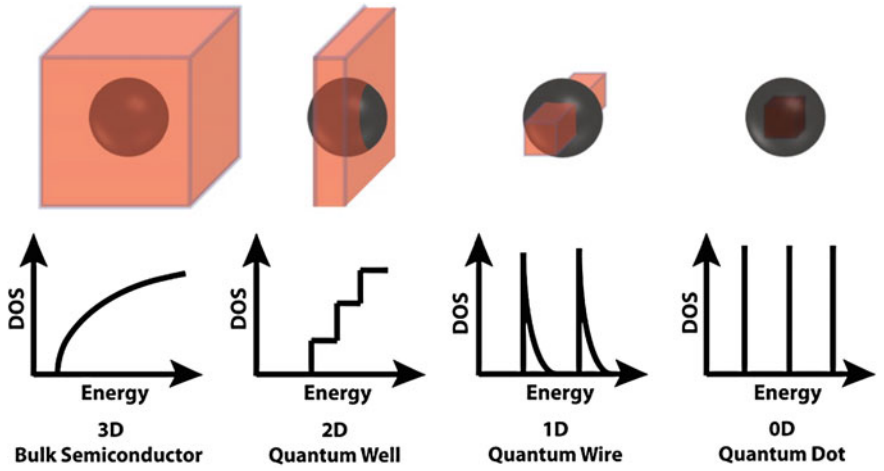

Fig. 2.11 Schematic illustration of the energy level structure of semiconductor nanostructures with reduced dimensionality(2D, 1D and 0D indicate two, one, or zero-dimensional, respectively) [3]. The energy level structure of a bulk semiconductor (3D) is shown for comparison. The exciton Bohr diameter is represented by the sphere. DOS gives the density of states

only in the thickness direction, a Quantum Well is formed (1-dimensional confinement). A schematic overview of the energy level structure of semiconductor nanostructures with reduced dimensionality is given in Fig. 2.11.

2.4.2 Nanocrystal as a Large Molecule: Building Up Atom by Atom

Another method to explain the unique properties of a quantum dot is based on a bottom-up approach [3, 16]. In this approach, the QD is seen as a large molecule or cluster. In analogy with quantum chemical methods for obtaining molecular orbitals (i.e. the Linear Combination of Atomic Orbitals, LCAO), the overall wave functions in a QD can be constructed from the individual atomic orbitals [3].

The simplest example of a multiple electron molecule is that of diatomic hydrogen (H_2). In this molecule, two atomic orbitals (AOs) combine to form two molecular orbitals (MOs) that spread out over both H atoms, namely a bonding and an anti-bonding MO. The bonding MO is lower in energy compared to the individual AOs, whereas the anti-bonding MO is higher in energy than the individual AOs. The MOs are occupied by electrons in such manner that the potential energy of the molecule is minimized. In the H_2 molecule the 2 electrons originally in the 1s AOs of the individual H atoms are accommodated in the bonding MO, thereby leaving the anti-bonding MO unoccupied. The highest occupied molecular orbital is referred to as HOMO and the lowest unoccupied molecular orbital is called LUMO.

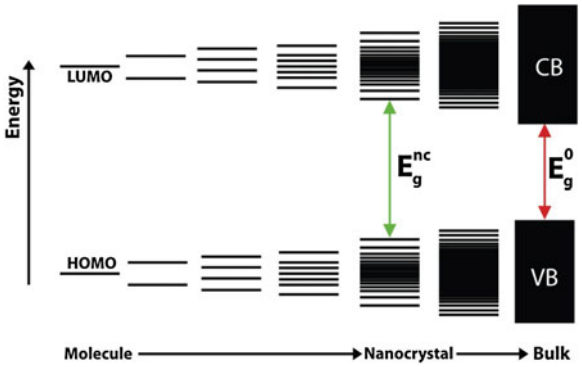

Fig. 2.12 Evolution of the energy level structure from a hypothetical diatomic molecule (*extreme left*) to a bulk semiconductor (*extreme right*). E_g^{nc} and E_g^0 indicate the energy gap between the highest occupied molecular orbital (HOMO) and the lowest unoccupied molecular orbital (LUMO) for a nanocrystal and bulk, respectively (CB = conduction band, VB = valence band). Reprinted with permission from Ref. [45]

The same approach can be extended to larger molecules, clusters and even bulk materials. As the molecule (e.g, a small CdSe cluster) becomes larger, the number of AOs that are combined to form MOs (bonding and anti-bonding) increases, leading to an increasingly larger number of energy levels and decreasing the HOMO-LUMO energy gap (Fig. 2.12). Each MO combination has a well-defined energy value, but MOs with intermediate energy values are more common than those with energies near the minimum or maximum values (i.e., fully bonding or fully anti-bonding). This means that the density of MO states is maximum at intermediate energy values, decreasing to a minimum at both energy extremes (i.e., highest and lowest). For a sufficiently large number of combining atoms (i.e., when the bulk limit is reached) the energy levels become so numerous and so closely spaced that a quasi-continuum (i.e., an energy band) is formed, analogous to the conduction and valence bands described above. The HOMO level is the top of the VB, whereas the LUMO is the bottom of the CB (Fig. 2.12).

A semiconductor NC can be regarded as a very large molecule or cluster consisting of a few tens to a few thousand atomic valence orbitals, forming as many MOs (for example, a 1.5 nm diameter CdSe NC contains about 50 atoms, while a 10 nm NC consists of 10^4 atoms). Therefore, its electronic structure will be characterized by energy bands with a large density of levels at intermediate energy values and discrete energy levels near the band edges, where the density of MO states is small. Moreover, the HOMO-LUMO energy gap will be larger than for bulk and size-dependent, increasing with decreasing size of the NC (Fig. 2.12). This explains both quantum confinement effects discussed in the previous section from a molecular point-of-view.

The MO approach described above provides a simple and general description of the electronic structure of a hypothetical 1-dimensional NC, and clearly illustrates the size dependence of the HOMO-LUMO gap. However, Fig. 2.12 presents the

evolution of the MOs that would be obtained from combining an increasingly larger number of identical AOs (i.e, with the same energy and symmetry). The situation for compound semiconductors (e.g, CdSe, CdTe, PbSe, InP) is more complicated since elements with different electronegativities and different types of AOs are combined. We will use the LCAO-approach in one dimension to describe the properties of a compound QD, using CdTe and CdSe as representative examples. The atomic structure of Cd, Te and Se are $[Kr]4d^{10}5\ s^2$, $[Kr]4d^{10}5\ s^25p^4$, and $[Ar]\ 3d^{10}4s^24p^4$, respectively. The electronic structure of CdTe and CdSe will thus be similar. In both cases the CB is comprised of linear combinations of the (empty) 5s atomic orbitals of Cd^{2+} [3], while the VB can be regarded as a linear combination of the (filled) sp^3 valence orbitals of Te^{2-} or Se^{2-}. For simplicity, we will neglect the sp^3 hybridization and consider that the VB is constructed from the p orbitals of Te or Se. It should be noted that this is an oversimplification, since p orbitals alone would not lead to the formation of a VB under the symmetry constraints imposed by the crystal structure of CdSe and CdTe (zinc blende or wurtzite), in which both the cation and the anion are tetrahedrally coordinated. Under this symmetry, the overlap between the p orbitals of the Se (or Te) anions would be too small. Nevertheless, this oversimplification is useful to illustrate the essential concepts behind the formation of bands from MOs, since in a hypothetical 1-d NC the overlap between the p-orbitals is sufficient to lead to band formation.

For a hypothetical single unit of CdTe the LUMO will be closer in energy to the 5s AOs of Cd, while the HOMO will be closer in energy to the 5p AOs of Te (Fig. 2.13a). As an increasingly larger number of units are combined in a hypothetical 1-dimensional CdTe crystal (constructed along the z-axis), the VB is progressively constructed from the π_y-like MOs resulting from the linear combinations of the $5p_y$ AOs of Te, whereas the CB is constructed from σ-like MOs resulting from the linear combinations of the 5 s AOs of Cd (Fig. 2.13b). Note that the

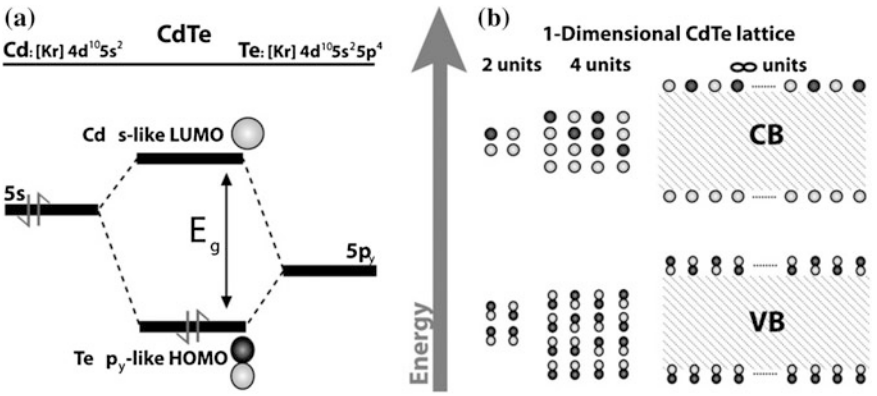

Fig. 2.13 **a** LCAO diagram of a hypothetical CdTe unit. **b** LCAO representation of n-units of CdTe. *Dark gray* and *light gray* indicate different phases of the MOs. Note the π-character of the valence band. Reprinted with permission from Ref. [19]

extremes of the bands consist of the most bonding and the most anti-bonding MOs. It should be pointed out that a similar π-band would emerge from the combination of the $5p_x$ AOs of Te. Since the degeneracy of the p-orbitals would not be lifted in a linear CdTe chain, the two π-bands would also be degenerate, and thus combine in a (hypothetical) π_{xy}-band extending over the whole 1-d CdTe NC. A σ-VB would also be formed from the linear combination of the $5p_z$ orbitals. Figure 2.14 schematically depicts the possible linear combinations of the p_z orbitals, using a hypothetical 1-dimensional CdSe crystal as an example. The MO diagram for a 1-d CdSe crystal is similar to that of CdTe, except that the VB emerges from the linear combinations of the 4p AOs of Se. A sinusoidal function that describes the phase (i.e. the sign of the amplitude) of each (hypothetical) σ-MO is also plotted in Fig. 2.14. The energetically most favourable combination takes place when the phase of each p-orbital changes sign at each selenium site, to form σ-bonding orbitals only. The linear combination of the Se 4p orbitals with the highest energy consists of p-orbitals that are all in phase (all anti-bonding). Similarly, the CB consists of linear combinations of the 5s-orbitals of Cd. The MO with the lowest energy is the linear combination of (bonding) s-orbitals that are all in phase, while the highest energy will be given by all the s orbitals out of phase.

At this point, it is instructive to compare the LCAO-approach with the Bloch-functions described above. The sinusoidal function describing the phase of the p-orbitals may be seen as the plane wave (e^{ikz}) of the Bloch function. As mentioned in Sect. 2.2, the fundamental band gap of CdSe is located at the Γ-point in the Brillouin zone. This means that the top of the valence band and the bottom of the conduction band are both situated at a k-value equal to zero. This is consistent with all the p-orbitals being in phase for the highest lying valence band level (HOMO), described by the sinusoidal function with the longest wavelength (i.e. smallest k). On the other hand, the lowest valence band level has the maximum k-value of π/a, which corresponds to all the p-orbitals changing phase at each selenium site (described by the sinusoidal function with the smallest wavelength). The periodic function ($u_k(z)$) in the Bloch-equation can be seen as the function describing the atomic orbitals; which is periodic over the lattice constant a because at each (selenium) site there is an identical atomic (p) orbital. Only the phase changes, which is described by the plane wave. A similar analysis can be carried out for the conduction band. The MO with the lowest energy is the linear combination of s-orbitals that are all in phase. The number of anti-bonding s-orbitals (and thus the energy) increases with increasing number of phase-flips (increasing k-value), and the conduction band level with the highest energy consists of a MO with only anti-bonding s-orbitals ($k = \pi/a$).

This 1-dimensional analysis is an oversimplification of the QD electronic structure, but it is helpful to understand the QD optical properties, since it shows that the nature of the orbitals constituting the VB and the CB is different. The discrete energy levels of the QDs can be related to different MOs, such as those shown in Fig. 2.14. Naturally, the number of MOs (and therefore of states) is much higher when all three dimensions are taken into account. The atomic-like symmetry of the band-edge levels (1S, 1P, etc.) is not apparent from the sinusoidal functions

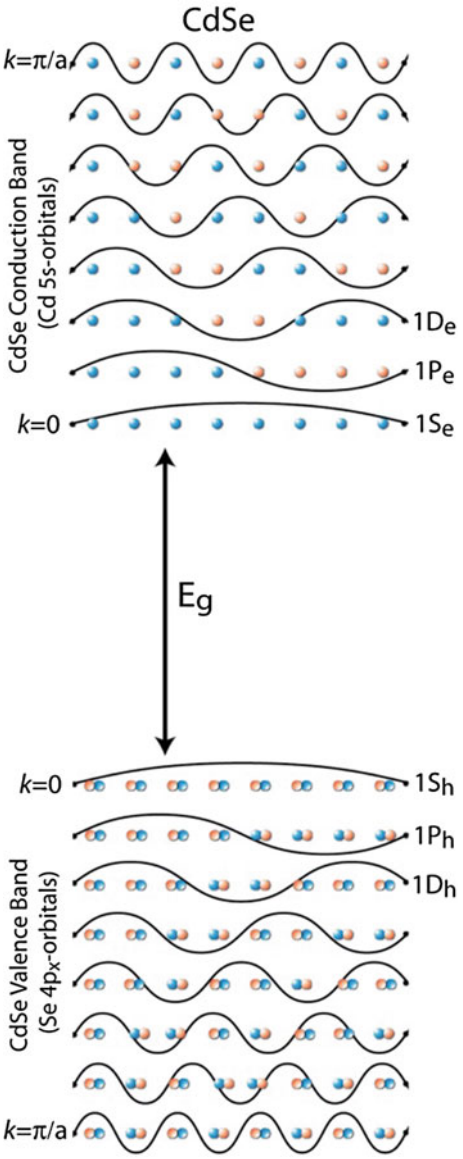

Fig. 2.14 LCAO-representation of the σ-MO levels in a one dimensional CdSe NC. The sinusoidal functions describe the phase of the atomic orbitals, and can be seen as the plane wave-part of the Bloch function. Reprinted with permission from Ref. [19]

(plane waves) in Fig. 2.14. However, it is clear that the probability of finding an electron at the edge of a QD (in real space) cannot be the same as in its centre. In this qualitative description, an envelope function (explained in the previous section) can be inserted to obtain the atomic-like symmetries for the band-edge MOs. When performing tight-binding or pseudo-potential calculations (based on the LCAO-approach), these atomic-like symmetries automatically arise from the boundary conditions that define the quantum dot [17, 18].

2.5 Optical Transitions in a Semiconductor Nanoparticle

As discussed above, the effect of quantum confinement is clearly observed in the optical properties of semiconductor nanostructures, causing a shift of all optical transitions to higher energies as the dimensions of the NC decrease (Figs. 2.1, 2.7, 2.8, 2.9). Moreover, the absorption spectra of QDs consist of a series of discrete peaks corresponding to optical transitions between different electron and hole levels of the QD (Figs. 2.7, 2.8, 2.9). As discussed in the sections above, the discrete energy levels of electrons and holes in semiconductor QDs are sequentially labelled as S, P, D, and so forth (Figs. 2.6, 2.7, 2.9). The optical transitions observed in the absorption spectra of QDs can thus be assigned to $1S_h$-$1S_e$, $1P_h$-$1P_e$, $1D_h$-$1D_e$, (and so forth, the subscripts h and e indicate hole and electron levels, respectively) electronic transitions.

To understand the optical transitions in semiconductor nanostructures (e.g., a quantum dot), we first look at what happens during an optical transition in the simpler case of a two level system [10]. In such an optical transition, an electron is excited from a ground state orbital $|1\rangle$ of the molecule to an excited state orbital $|2\rangle$. The underlying process of the excitation is the mixing of the ground state and excited state orbitals into a combined (mixed) state $(\psi = c_1|1\rangle + c_2|2\rangle)$. This mixing of the two orbitals is induced by the oscillating electric field of an incoming electromagnetic (EM) wave (photon), and can only take place if the mixed state has a dipole moment. The two wave functions are mixed because of a distortion (polarization) caused by the oscillating electric field of a photon, which can only happen if a dipole moment is induced in the mixed state, and if the frequency of the EM field corresponds to the frequency difference between the two states. Figure 2.15 shows what happens when different orbitals (with different phases) are combined. It is clear that two orbitals with the same parity combine into a symmetric mixed wave function, without a dipole moment. Mixing of these orbitals cannot be induced by an oscillating electric field. On the other hand, when two orbitals with a different parity are mixed, the net result is an orbital with a dipole moment [10]. In summary, optical transitions in atoms or molecules can only occur between orbitals with a different parity (e.g., s $\rightarrow$ p, p $\rightarrow$ s, or p $\rightarrow$ d, etc.). This is known as the parity selection rule ($\Delta\ell = \pm 1$). In the treatment below, we focus only on this selection rule. Other selection rules, such as the spin selection rule, are not considered.

Let us now consider the (coherent) excitation of an electron from the 1s to 1p orbitals in a hydrogen atom. During excitation, the combined state of the 1s and 1p orbitals (with a net dipole moment, see Fig. 2.15) [19] starts to oscillate with the frequency of the EM field, and by doing so, the states become more and more mixed. Note that this only happens when the frequency of the incoming wave is resonant with the *eigen*-frequency of the oscillating dipole (in other words, when the energy of the photon matches the energy difference between the ground and excited state). Initially, the mixed state has mainly 1s-character $(\psi = c_1|1\rangle + c_2|2\rangle)$ with $c_1 \gg c_2$). After a certain number of oscillations (typically $\sim 10^8$ for a

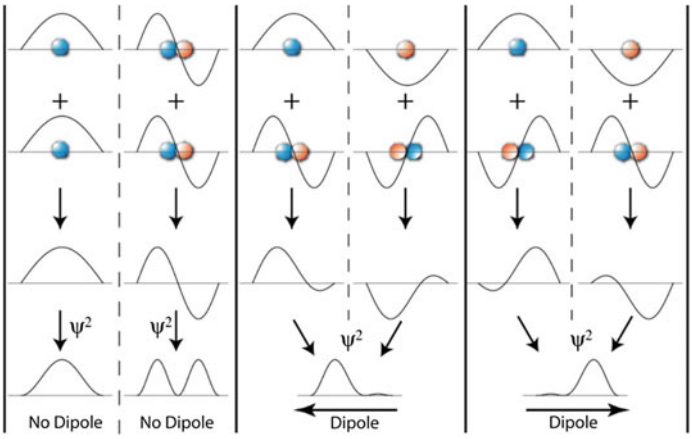

Fig. 2.15 Schematic representation of the linear combination of s and p orbitals. When two s or two p orbitals are mixed (*left*), a symmetric wave function results without a dipole moment. Mixing of an s and p orbital (*middle* and *right*) results in an asymmetric wave function with a dipole moment, the direction of which depends on the phase of the original wave functions. Reprinted with permission from Ref. [19]

molecule, depending on the intensity of the EM field) [20] the s and p orbitals are in the maximally mixed state ($c_1 = c_2$) (Fig. 2.15, middle and right panels). After this, the mixed state becomes more and more p-like, and after again $\sim 10^8$ oscillations the state has purely p-character ($c_1 = 0$ and $c_2 = 1$); i.e., the excitation is complete. However, the oscillations can continue, to go back to the maximally mixed state and finally the pure s-state again (which can be regarded as stimulated emission, see below). The complete cycle from 1S to 1P states and back to the 1S-state is called the Rabi-cycle, and is a fully coherent process. The coherent excitation from the ground state (1S) to the excited state (1P) takes half of the Rabi-cycle, which typically involves $\sim 10^8$ oscillations of the EM field (~ 10 ns). In practice, excitation (using an incoherent light source) in atoms or molecules is incoherent, which means that already after a few oscillations ($\ll$ps), the mixed state collapses (decoheres) to either the ground state or excited state.

What about an optical transition in a quantum dot? We will use the bottom-up (LCAO) approach to analyse the optical transitions and corresponding selection rules in a QD. In contrast to the case of a hydrogen atom, electrons in a QD (e.g. CdSe) occupy molecular orbitals (MOs). Therefore, we have to consider optical transitions between two MOs in a QD. The lowest energy interband transition is between the lowest hole level ($1S_h$) and lowest electron level ($1S_e$) (see Fig. 2.9 above). As illustrated in Fig. 2.16a, this involves a transition from a MO formed by the linear combination of Se 4p-orbitals to an MO formed by the linear combination of Cd 5s orbitals. Within each unit cell, mixing of these states yields a dipole moment (indicated by the small arrows in Fig. 2.16). Because the atomic orbitals are all in phase ($k = 0$), all the dipoles of the individual unit cells point in the same direction. Note that the length scale of the collection of individual dipoles (a few

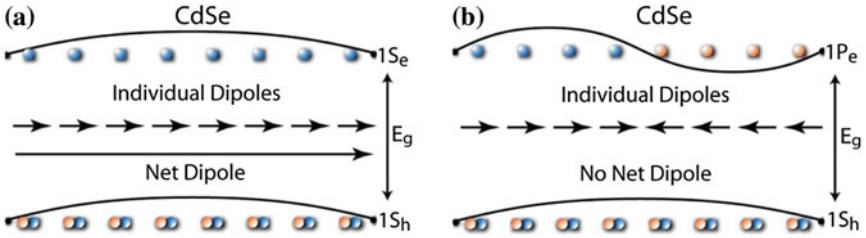

Fig. 2.16 Schematic representations of the individual dipoles and net dipole moments that arise when VB atomic orbitals are mixed with CB orbitals, for three different interband transitions in a CdSe QD. The direction of the individual dipole can be deduced from Fig. 2.15. When the individual dipoles add up to a net dipole, the optical transition is parity-allowed. If they cancel out (B), the transition is parity-forbidden. Reprinted with permission from Ref. [19]

nm) is much smaller than the wavelength of the excitation light (e.g., ~500 nm). Therefore, the individual dipoles all experience the same oscillating field of the incoming EM wave. As a result, the individual dipoles add up to a total net dipole moment of the two mixed MOs, making the $1S_h$-$1S_e$ optical transition parity-allowed. The same reasoning applies to any other interband transition involving electron and hole states of the same parity, such as $1P_h$-$1P_e$ or $1D_h$-$1D_e$, which are all parity-allowed.

The situation is different for interband transitions between electron and hole states of different parity, such as $1S_h$-$1P_e$ or $1S_h$-$1D_e$, which are strongly parity-forbidden and are therefore never observed in the absorption spectrum of QDs. In this case, the direction of the individual dipoles changes half-way of the QD (in real space) because of the phase-shift in the 5s-orbitals in the conduction band (Fig. 2.16b). The individual dipoles now cancel out yielding a net dipole moment of zero (i.e., no dipole). Therefore, the $1S_h$-$1P_e$ interband optical transition is not allowed. From these examples, we see that the selection rule for an optical interband transition in a quantum dot is $\Delta L = 0$ for the envelope-wave functions. The parity-selection rule is still obeyed in e.g. a CdSe QD, because the interband transition involves the transition from (a linear combination of) 4p orbitals to (a linear combination of) 5s orbitals, which have different parities (viz., 1 and 0, respectively, thus $\Delta\ell = 1$).

Optical transitions in semiconductor nanostructures can also take place between different electron levels or different hole levels (e.g., $1S_e$-$1P_e$). These transitions are referred to as intraband transitions. For an intraband transition, a similar treatment can be used to obtain the optical selection rules. These transitions involve MOs consisting of different combinations of the same type of atomic orbitals (e.g., Cd 5s for the electron levels of CdSe QDs). In this case $\Delta\ell = 0$ for the atomic orbitals and no dipoles will arise within the individual unit cells (Fig. 2.15). Therefore, the dipole has to arise from a change in parity of the envelope functions ($\Delta L = \pm 1$), which means that for example the $1S_e$ to $1P_e$ intraband transition is parity-allowed, whereas the $1S_e$-$1D_e$ transition is forbidden. The net dipole arises because half of the 5s-orbitals (that are in phase) add up, whereas the other half of the 5s-orbitals

cancel out because they have a different phase. This causes an asymmetric electron density distribution in the quantum dot when the $1S_e$ and $1P_e$ levels are mixed, giving rise to a net dipole, which makes the transition parity-allowed.

2.6 Exciton Relaxation and Recombination

Exciton Relaxation. After absorption of a photon by a semiconductor NC (e.g., a quantum dot or quantum rod) an exciton is created, with the electron and hole occupying one of the discrete energy levels available within the conduction and valence bands. If the energy of the photon is sufficiently large a hot exciton is formed, in which the electron and hole occupy excited states (i.e., states above the 1S level). In such a case, the electron and hole will quickly (<1 ps) relax to their ground states (the $1S_e1S_h$ exciton) by means of a cascade of intraband non-radiative relaxation steps, through which their excess energy is dissipated as heat [6]. These radiationless intraband transitions are not constrained by the optical selection rules mentioned above, and therefore can take place very fast, either by coupling with phonons (i.e., lattice or ligand vibrations) of suitable energy, or by Auger scattering processes through which the excess energy of one carrier (e.g., the electron) is transferred to the other (e.g., the hole) [6, 9].

Exciton Recombination. Once the exciton has reached its ground state (i.e., the lowest energy $1S_e1S_h$ exciton), further relaxation can only take place by electron-hole recombination, through which the excited electron returns to the valence band and the exciton energy is released either radiatively or non-radiatively (Fig. 2.17) [10].

Radiative recombination results in the emission of a photon. In the emission spectra of QDs (and quantum rods) the direct radiative recombination of the exciton is observed as a well-defined peak with energy close to the lowest energy absorption transition. The emission peak position presents thus the same size

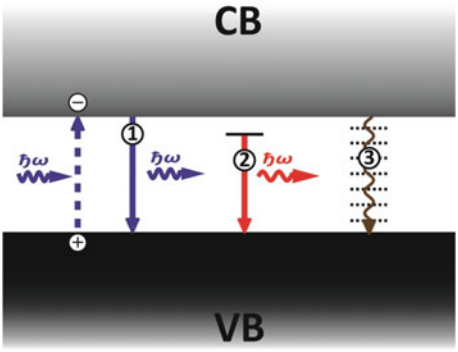

Fig. 2.17 Schematic illustration of exciton recombination pathways in semiconductors. *1* radiative recombination. *2* defect assisted radiative recombination. *3* non-radiative recombination. Reprinted with permission from Ref. [45]

dependence as the absorption transitions. The peak widthsare determined primarily by the size and shape distribution of the ensemble of NCs investigated (inhomogeneous line broadening).

It should be noted that the emission transition is just the reverse of the lowest energy absorption transition. Therefore, the selections rules discussed above for absorption also apply for emission. Emission of a photon results from the mixing of the excited state orbital with the ground state orbital. This mixing also has to be induced by an external oscillating field. Without this external "trigger", an electron can theoretically reside in the excited state for an infinite time. An incoming EM wave that is resonant with the transition can induce the mixing (just as in case of absorption) resulting in radiative recombination. This is called stimulated emission, which is used in lasers.

Usually, the fluorescence of dyes, phosphors, and quantum dots takes place without the stimulus of an external oscillating field. In that case one speaks of spontaneous emission, where mixing of the excited and ground state is induced by so-called vacuum modes (or vacuum fluctuations). The rate of spontaneous emission is not only dependent on the magnitude of the transition dipole moment $\mu_{i,f}$ between initial and final states (proportional to the oscillator strength), but also on the density of optical modes that can couple to the transition. The density of optical modes in vacuum is frequency-dependent and increases with frequency. The radiative decay rate Γ_{rad} for spontaneous emission in an ideal two-level atom system can be deduced from Fermi's Golden Rule [10, 21] and contains both the "atomic" part (transition dipole moment) and "field" part (density of optical modes):

$$\Gamma_{rad}(\omega) = \frac{\omega^3 n \left|\mu_{i,f}\right|^2}{3\pi\varepsilon_0 \hbar c^3} \tag{2.15}$$

where ω is the frequency of light, n is the refractive index, ε_0 is the permittivity of free space, and c is the speed of light. The rate of spontaneous emission can be modified by changing the density of optical modes, which can be achieved in photonic crystals [21].

Non-Radiative Exciton Recombination is usually mediated by defects or impurities, since the dissipation of the exciton energy by coupling to phonons (vibrations) requires the simultaneous creation of a large number of phonons (>50 for CdSe QDs), making it a very unlikely process. On the other hand, trapping (i.e., localization) of one of the charge carriers at a defect or surface state (trap states) is a much faster process, which can efficiently compete with radiative recombination, resulting in quenching of the exciton emission. Trapping leads to strong carrier localization, which decreases the overlap between the electron and hole wave functions, thereby making the radiative recombination less likely and facilitating non-radiative relaxation by coupling to local vibrations. Radiative recombination can still occur if the exciton is trapped in a defect or surface state, but this will lead to a broad emission band at lower energies than the band gap (trap or defect related

luminescence), which is typically very inefficient (photoluminescence quantum yields below 5 %) [2]. The surface is the most important source of trap states in NCs. As discussed in Chap. 1, surface atoms have fewer neighbours than their interior counterparts, and therefore possess unsatisfied chemical bonds (dangling bonds). These unshared atomic orbitals give rise to energy levels within the HOMO-LUMO gap of the semiconductor NC (surface states) [3]. Surface defects (e.g., vacancies) give rise to even more strongly localized energy states, which can very effectively trap the electron or hole. For these reasons, it is essential to control the surface quality of semiconductor NCs and eliminate dangling bonds, a process known as surface passivation. This can be achieved either by overgrowing a shell of a wider band gap semiconductor or by coating the surface with suitable organic ligands (Chap. 6) [2].

Exciton Energy Transfer. Another possible non-radiative recombination pathway is energy transfer between QDs. When two QDs are in close proximity, an exciton in one QD (donor) can be transferred to a neighbouring QD (acceptor) through a dipole-dipole interaction [22]. This process is called resonant exciton energy transfer (ET), and is an alternative pathway for an exciton in the donor QD to recombine. Exciton ET should not be confused with radiative ET, where a QD re-absorbs light that was emitted by another QD. Classically, resonant ET can be seen as an oscillator that induces a neighbouring oscillator (with the same resonance frequency) to oscillate as well. In the case of exciton ET, the oscillating dipole in a donor QD induces the oscillation of a dipole in the acceptor QD. Through this dipole-dipole interaction, the energy of the exciton in the donor QD can be transferred to the acceptor QD. The net result is a physical displacement of the exciton from the donor QD to the neighbouring acceptor QD (Fig. 2.18), which is not mediated by an external EM field. Exciton ET between neighbouring QDs can be studied by using (time-resolved) fluorescence spectroscopy, through which the emission decay functions of the donor and acceptor QDs are followed (see below).

Several conditions must be satisfied for exciton ET to occur [22]. First, the distance between the two QDs must be sufficiently small. Secondly, the (absorp-

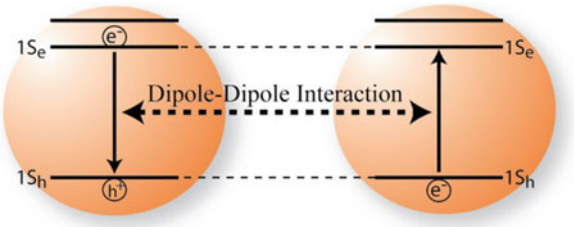

Fig. 2.18 Schematic representation of resonant exciton energy transfer from the donor QD (*left*) to the acceptor QD. The exciton in the donor QD recombines, inducing an exciton in the acceptor QD through a dipole-dipole interaction. Reprinted with permission from Ref. [19]

tion) transition of the acceptor QD must be resonant with the (emission) transition of the donor QD (i.e., there must be spectral overlap). This implies that the band gap of the acceptor QD has to be equal to or smaller than the band gap of the donor QD (ET to higher-lying levels in the acceptor QD is also possible). Finally, the orientation of the oscillating dipoles in both QDs also influences the transfer rate. Based on these conditions, the total energy transfer rate (Γ_{ET}) can be written as:

$$\Gamma_{ET} = \frac{2\pi}{\hbar}\frac{\mu_D^2\mu_A^2\kappa^2}{r^6 n^4}\Theta \tag{2.16}$$

as was first derived by Förster [23], where μ_D and μ_A denote the transition dipole moments of the donor and acceptor quantum dot respectively, r is the distance between the (centre of) the dipoles, and n is the refractive index of the surrounding medium. This r^{-6} distance dependence is only valid when r is larger than l, where l is the length of the dipole ($l = \mu/q$, q is the elemental charge). The orientational average of the dipoles κ in quantum dots is 2/3, assuming that the dipoles are randomly oriented. The spectral overlap is represented by Θ, which is defined as:

$$\Theta = \int E_D(\lambda) \cdot A_A(\lambda) d\lambda \tag{2.17}$$

where $E_D(\lambda)$ is the (normalized) emission spectrum of the donor QD, and $A_A(\lambda)$ represents the (normalized) absorption spectrum of the acceptor QD.

Exciton Lifetime. The lifetime of an exciton in a semiconductor QD can be determined by measuring the photoluminescence (PL) decay times τ, and can be described as

$$\tau = \frac{1}{W_{TOT}} = \frac{1}{W_{Rad}} + \frac{1}{W_{NRad}} + \frac{1}{W_{ET}} \tag{2.18}$$

where W_{TOT} is the total decay rate, W_{Rad} is the radiative decay rate, W_{NRad} the non-radiative decay rate, and W_{ET} the energy transfer rate. The latter can be neglected for a sufficiently diluted solution of QDs. If the excitons in a system decay only radiatively, the PL decay will follow a single exponential behaviour:

$$N(t) = N_0 e^{-t/\tau} \tag{2.19}$$

where t is the elapsed time after the excitation, τ is the exciton radiative lifetime and N_0 is the population of the emitting state at t = 0, which determines the PL intensity at t = 0. When non-radiative recombination and energy transfer contribute to the exciton relaxation, the PL decay will no longer follow a single exponential behaviour. The total decay rate will then contain different contributions and therefore the PL decay curves will show a multiexponential behaviour. The balance between the radiative and non-radiative decay rates will be reflected in the PL quantum yield (PL QY), which is the ratio between the number of emitted (n_{em}) and absorbed (n_{abs}) photons, as given by:

$$QY = \frac{n_{em}}{n_{abs}} = \frac{W_{Rad}}{W_{TOT}} \tag{2.20}$$

2.7 Excitons in Semiconductor Heteronanostructures

The ability to create novel optoelectronic properties can be extended further by using semiconductor heteronanocrystals (HNCs) instead of single composition NCs. HNCs are comprised of two (or more) different materials joined in the same particle by one or more heterointerfaces (see Chap. 6 for details) [2]. The energy level alignment between the materials that are combined at the heterojunction is of paramount importance. Depending on the energy offsets between the HOMO and the LUMO levels of the two adjoining materials, different charge carrier localization regimes will be observed after photoexcitation. Three limiting cases can be identified: type-I, type-$I^{1/2}$ (also referred to as *quasi*-type-II) and type-II (Fig. 2.19) [2]. In the **Type-I regime** the band gap of one semiconductor lies entirely within the gap of the other material. Therefore, after photoexcitation electron (e) and hole (h) are confined primarily in the same part of the HNC (the narrower gap material), resulting in a **direct exciton**. In the **Type-II regime** the staggered energy level alignment results in the spatial separation of the electron and hole on different sides of the heterojunction, leading to the formation of a **spatially indirect exciton**. In the **Type-$I^{1/2}$ regime** one carrier is confined in one of the components, while the other is delocalized over the whole HNC.

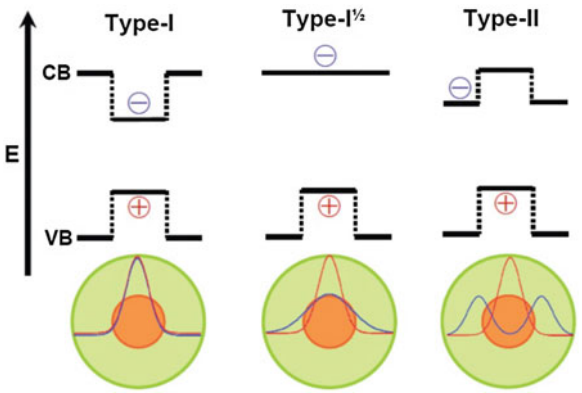

Fig. 2.19 Schematic representation of the three limiting charge carrier localization regimes incore/shell semiconductor HNCs. The conduction and valence band edges (i.e., the LUMO and HOMO energy levels) are indicated by CB and VB, respectively. The *plus* and *minus* signs represent the charge carriers (hole and electron, respectively). The electron and hole ground-state wave functions are schematically depicted in the *lower panel*. Reproduced by permission of the Royal Society of Chemistry from Ref. [2]

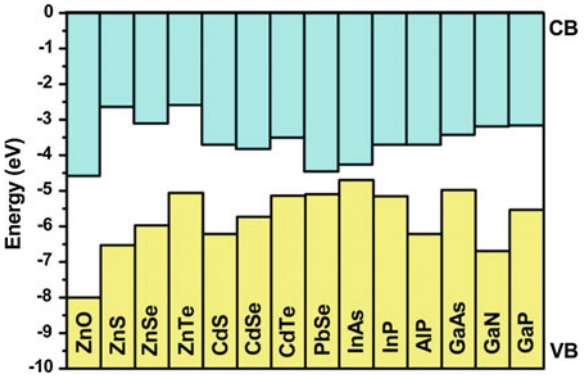

Fig. 2.20 The energy of the electronic band edges relative to the vacuum level of selected semiconductors (VB: valence band, CB: conduction band). The space between the *solid bars* gives the band gap. Bulk values are used, except for PbSe, which have been estimated from NC results. Reproduced by permission of the Royal Society of Chemistry from Ref. [2]

The band offsets in the bulk limit can be obtained from the band positions of the bulk semiconductors, which are known only for a limited number of materials (Fig. 2.20). The nanoscale dimensions of HNCs can be exploited to further expand the gamut of properties originating from a given combination of materials. Since the position and the density of energy states in quantum confined semiconductor nanostructures is governed by size and dimensionality (Sect. 2.4), the energy offsets in semiconductor HNCs can be tuned by a judicious control of the composition, size and shape of each component. This offers the possibility of directly controlling the *e-h* wave function overlap, thereby tailoring the material optoelectronic properties. This flexibility in engineering the properties of colloidal HNCs has important consequences for a number of technologies, and opens up interesting application possibilities: low-threshold lasers, light-emitting diodes, photovoltaic devices, fast optical switches, IR detectors, fast access memories, spintronic devices, and labels for biomedical imaging [2]. An overview of the properties associated with each type of HNC will be given below.

Type-I HNCs. Type-I concentric core/shell QDs (e.g., CdSe/ZnS, CdS/ZnS, InP/ZnS) are the most investigated colloidal semiconductor HNCs [2, 24]. This large interest stems from the fact that the exciton is confined to the core, and therefore is protected from interaction with the surface and the environment. Moreover, the exciton no longer probes dangling orbitals since the interface core atoms are bound to the shell atoms. Consequently, the photoluminescence quantum yields are high (≥50 %) and the stability against photodegradation is enhanced [24]. The properties of a direct exciton in a type-I HNC are dictated primarily by the narrow gap material. This means that upon the shell overgrowth the emission and absorption spectra of the core should remain unaffected, except for the appearance of new high energy absorption peaks associated with the shell material. However, the energy offsets between the two materials are finite and therefore the exciton wave function partially

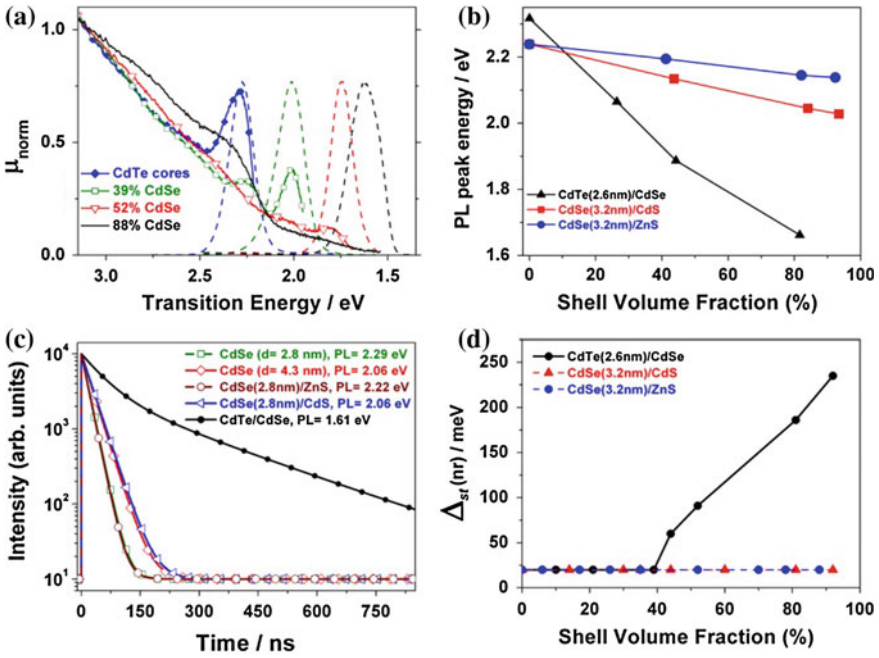

Fig. 2.21 **a** Photoluminescence (PL, *dashed lines*) and PL excitation (PLE, *solid lines*) spectra of colloidal CdTe/CdSe HNCs with a 2.6 nm CdTe core and increasing CdSe volume fraction (39–88 %). PL spectra are normalized at the peak. PLE spectra are normalized to 1 at 3.1 eV. The symbol μ_{norm} gives the normalized absorption cross section per Cd(Te, Se) ion pair unit. The evolution from Type-$I^{1/2}$ (39 % CdSe) to Type-II (88 % CdSe) localization regimes is clearly observed. **b** PL peak position of colloidal core/shell HNCs of different compositions as a function of the shell volume fraction. The diameter of the core NC is indicated between brackets. The compositions were chosen as representative examples of different carrier localization regimes (viz., Type-I: CdSe/ZnS; Type-$I^{1/2}$: CdSe/CdS, CdTe/thin shell CdSe; Type-II: CdTe/thick shell CdSe). **c** PL decay curves of CdSe QDs and three different core/shell HNCs. To facilitate comparison, only the initial 850 ns of the decay curve of CdTe/CdSe HNCs are shown. (d) Non-resonant Stokes shift ($\Delta_{ST}(nr)$) as a function of the shell volume fraction for different core/shell HNCs (viz., Type-I: CdSe/ZnS; Type-$I^{1/2}$: CdSe/CdS, CdTe/thin shell CdSe; Type-II: CdTe/thick shell CdSe). Reproduced by permission of the Royal Society of Chemistry from Ref. [2]

extends into the shell (this is usually referred to as "exciton leakage"). Consequently, a small (i.e., ≤50 meV) redshift is observed for all exciton transitions, both in emission and absorption (see, e.g., CdSe/ZnS) [2] (Fig. 2.21). The redshift is proportional to the reduction in exciton confinement and therefore is larger for smaller offsets. The energy difference between the maxima of the emission band and of the lowest energy absorption band (the so-called "non-resonant Stokes shift") is not affected, and remains ≤20 meV [2] (Fig. 2.21). The exciton radiative lifetime also remains essentially the same (Fig. 2.21), although the observed photoluminescence decay time will typically be longer, due to the reduction of the non-radiative recombination rates, since the exciton no longer probes the surface [2].

In practice, the exciton leakage into the shell implies that thick shells (and larger offsets) are needed to effectively prevent the exciton from probing the surface. However, interfacial strain induced by lattice mismatch between the core and shell materials becomes a serious issue for thick shells, and may severely limit the maximum thickness [2, 24]. For example, from the viewpoint of energy offsets, ZnS is the best shell material for CdSe based core/shell QDs, but the large lattice mismatch (12 %) makes it difficult to grow shells thicker than 2–3 monolayers (MLs). ZnSe and CdS give smaller lattice mismatches (6.3 and 3.9 %, respectively), but also smaller energy offsets. The solution is to grow multiple shells of different compositions around a central core, so that the energy offsets progressively increase towards the surface, but with small lattice mismatches between subsequent shells (e.g., CdSe/CdS/(Cd,Zn)S/ZnS core/multishell QDs [24]). Shell growth strategies are discussed in detail in Chap. 6.

Type-I$^{1/2}$ HNCs. The most investigated Type-I$^{1/2}$ HNC composition is CdSe/CdS, although it is usually referred to as a "Type-I" core/shell QD. However, it is well established that the energy offset for the electron is too small to confine it to the CdSe core, and, consequently, the electron wave function may delocalize over the entire HNC, while the hole remains confined in the CdSe core [25]. Other examples of Type-I$^{1/2}$ HNCs are ZnSe/CdSe core/shell QDs (*e* localized in CdSe shell, *h* delocalized over the HNC) [26], CdTe/CdSe core/thin shell HNCs (*h* is confined to core, *e* is delocalized) [27], and PbSe/CdSe core/thin shell QDs (*h* in core, *e* delocalized) [28]. The redshift observed in the PL and absorption spectra upon shell overgrowth (viz., up to 200–400 meV, depending on the core diameter) is much larger than that observed for Type-I HNCs, due to the loss in confinement energy of the carrier that is delocalized over the entire volume of the HNC [27] (Fig. 2.21). The Stokes shift, however, remains small (≤20 meV) and is comparable to that observed for single component NCs and Type-I HNCs [27] (Fig. 2.21). The absorption peaks remain distinct and well-defined, in contrast to the behaviour observed for Type-II HNCs (see below) [25, 27]. The delocalization of one of the carriers reduces the *e*-*h* overlap, leading to longer exciton radiative lifetimes (Fig. 2.21). The PL QYs can be as high as 80 % [2, 24–27].

Type-II HNCs. The properties of the spatially indirect exciton can be manipulated by choosing suitable combinations of semiconductors [2, 24–27]. It should be noted that complete spatial separation occurs only for the physically unrealistic case of infinite offsets. For finite offsets the wave functions of the carriers partially extend across the heterojunction, leading to non-zero *e*-*h* overlap. The indirect nature of the exciton leads to longer radiative lifetimes [2, 26, 27], increased exciton polarisability [26], and emission at lower energies than those of the band-gaps of both materials [2], thus allowing access to wavelengths that would otherwise not be available. It has also been reported to make single exciton lasing possible [29]. Further, the rates for hot carrier relaxation [30] and spin flip [31] decrease, as a consequence of the (partial) spatial separation of the photoexcited charge carriers. The potential of colloidal type-II HNCs has attracted increasing attention over the last few years, leading to the investigation of HNCs of various compositions (viz.,

CdTe-CdSe, CdSe-ZnTe, ZnTe-ZnSe, and ZnSe-CdS) and shapes (viz., core/shell NCs, rods and multipods, and dumbbells) [2].

The redshift observed in the PL and absorption spectra upon shell overgrowth is very large (e.g., up to 0.5–0.8 eV for CdTe/CdSe HNCs, depending on the CdTe core diameter) [2, 27, 32] (Fig. 2.21), making Type-II HNCs promising near-IR emitters. It should be noted that thick shells (>1 nm) are needed to achieve the Type-II localization regime [2, 26, 27]. Thin shells yield Type-$I^{1/2}$ HNCs. The onset of the Type-II regime is characterized by the loss of structure of the lowest energy absorption band (i.e., a featureless absorption tail develops), accompanied by a simultaneous increase in the Stokes shift (up to 200–300 meV) and bandwidths [2, 27] (Fig. 2.21). Also, the absorption cross section at emission energies decreases dramatically and the exciton radiative lifetime becomes much longer (0.2–2 μs, 1–2 orders of magnitude longer than that of a direct exciton in the same materials) [2, 27] (Fig. 2.21).

2.8 Size Effects on the Electronic Structure of Nanocrystals: Semiconductors in Comparison to Metals

As discussed in Chap. 1, the optical properties ofmetal NCs may also be strongly size dependent. This is particularly evident for gold, as clearly illustrated in Fig. 1.1 (Chap. 1), 2.22, and 3.4 (Chap. 3). Nevertheless, the wide range of colours observed for suspensions of gold NCs cannot be ascribed to quantum confinement effects [3]. Since the highest energy band in metals is partially occupied, the Fermi level lies close to the centre of the band. As shown in Fig. 2.12 above, the density of states (and the energy level spacing) near the centre of the bands is only affected when the

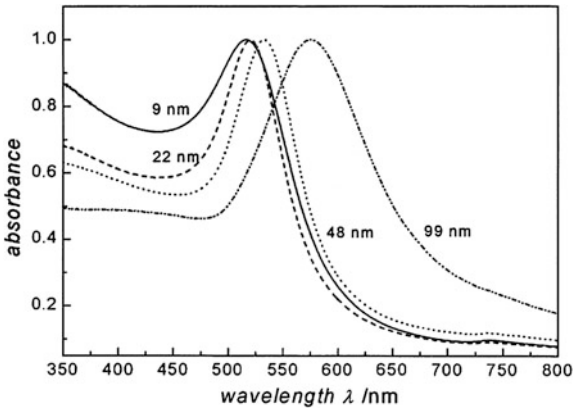

Fig. 2.22 Absorption spectra of colloidal suspensions of gold NCs in water (diameters: 9, 22, 48 and 99 nm). The spectra are normalized at their maxima (517, 521, 533, and 575 nm, respectively). Reprinted with permission from [47], Copyright (1999) American Chemical Society

NC size approaches the cluster size regime. As a result, the electrical and optical properties of metal NCs will be affected by quantum confinement effects only when the dimensions of the NC become comparable to or smaller than the Fermi wavelength in the metal (<2 nm for all metals). To understand the size dependence of the optical properties of metal NCs and nanostructures larger than 2 nm, one has to consider the impact of spatial confinement on the plasmon resonances of metals. This will be addressed in detail in Chap. 3.

2.9 Applications of Semiconductor Nanoparticles

The unique size- and shape-dependent optoelectronic properties of semiconductor nanostructures can be exploited in many different applications. The field is currently developing at an astounding pace, and it is therefore not possible to present here a comprehensive overview of all the current and potential applications of semiconductor NCs. We will instead limit ourselves to sketch the state-of-the-art on a number of applications, highlighting the specific properties of semiconductor nanoparticles that make them attractive for a particular application. This section should be regarded as a blurred snapshot of a fast-moving object and, as such, bound to change soon, as far as the details are concerned.

Epitaxial and colloidal nanostructures. As discussed above (Sect. 2.4.1.1), semiconductor nanostructures (NSs: QDs, Quantum Wells, Quantum Wires) can be classified in "Colloidal" and "Epitaxial" depending on their synthesis method. Epitaxial NSs are prepared by relatively high-energy input vapour phase methods, which require ultrahigh-vacuum environments and extremely high purity chemical precursors. In contrast, colloidal NSs are prepared by solution based approaches ('wet' chemistry) that are relatively inexpensive, facile, scalable, and less sensitive to impurities (see Chap. 6 for details). The size and shape control offered by colloidal techniques are unmatched by epitaxial techniques, which typically yield NSs in the weak quantum confinement regime, owing to their relatively large lateral dimensions (>10 nm) [33]. Moreover, epitaxial NSs are substrate-bound, which makes their integration into electronic devices easier, but severely limits their applicability. In contrast, colloidal NSs can easily be subjected to post-synthesis procedures, such as size-selection and surface functionalization, and can be solution-processed into thin-film assemblies and composites (see Chaps. 1 and 6 for details).

Lasers. The density of states near the band edge increases in NSs as a result of quantum confinement (Fig. 2.11 above). This effect becomes more and more pronounced as the dimensionality of the active layer is further reduced, so that injected charge carriers concentrate in an increasingly narrower energy range near the band edge. As a result, the maximum material gain increases and the temperature dependence of laser parameters is reduced [34]. Moreover, quantum confinement effects considerably extend the wavelength tunability. The superior performance of lasers based on semiconductor nanostructures has led to a number commercial

devices based on dense ensembles (10^{10} cm^{-2}) of epitaxial QDs as the active layer. These lasers show excellent thermal, temporal, and spatial stabilities, and large radiation resistance [34]. Low-threshold lasing has also been observed in colloidal QDs [35], but devices have yet to be demonstrated, although much progress has been made in recent years [36].

Optical amplifiers. Devices based on dense ensembles of epitaxial QDs are also effective as low-cost optical amplifiers and signal regenerators in all-optical networks, and promise superior performance in comparison with devices based on quantum wells and bulk media owing to its inherently faster gain recovery and broader bandwidth [34].

Single-photon source. Single-QD devices are compact and easy to integrate into existing technology, making them attractive for applications in quantum information processing, where they can fulfil the roles of both single-photon emitters and quantum memory by storing the polarization state of a single photon [34].

Light emitting devices. The bright, spectrally narrow, and tunable luminescence of colloidal QDs makes them outstanding sources of saturated emission colours for light emitting devices (LEDs) and displays, since these properties allow for wider colour gamut, larger colour rendering index, and high luminous efficiency [33, 36]. Moreover, colloidal QDs (cQDs) are stable and solution processable, enabling the use of low-cost deposition techniques such as spin-coating, inkjet printing, or microcontact printing [33]. They are therefore promising materials for light-weight flexible displays, offering an alternative for Organic LED's (OLEDs). The performance of electrically driven cQD-LEDs has improved dramatically over the last decade, reaching in 2013 peak external quantum efficiencies (EQE) of 18 % and brightness values of 3×10^4 cd m^{-2} [33]. At the time of writing, these values were still below those of OLEDs (viz., 25 % and 8×10^4 cd m^{-2}), but were increasing steadily, indicating that cQD-LEDs may still become a serious competitor for OLEDs. Nevertheless, there are still many challenges to be addressed before cQD-LEDs become an accepted and viable technology (viz., lifetimes are only 100–1,000 h, operating mechanisms are poorly understood, most efficient devices are based on heavy metal based QDs, such as CdSe) [33, 36].

Biomedical imaging applications. One of the most rapidly developing applications of nanotechnology in biomedical research is the use of colloidal nanoparticles as contrast agents and luminescent labels for (in vivo) biomedical imaging [37]. For example, iron oxide NCs can be used as contrast agents for MRI (Magnetic Resonance Imaging), and gold NCs are suitable contrast agents for Computed Tomography (CT). Colloidal QDs exhibit a number of exceptional optical properties compared to fluorescent dyes, which greatly enhances their potential as labels in fluorescence based bio-imaging. The most significant properties include: (1) broad and strong absorption (2) narrow and symmetric photoluminescence spectra with high quantum yields, and (3) high resistance to photobleaching and chemical degradation. In addition, the surface of colloidal QDs can be functionalized with molecules that improve pharmacokinetics and bio-applicability, or target specific biomolecules. Interestingly, new developments allow the creation of QD-based nanoparticles that can be detected with several imaging techniques, so-called multimodal QDs.

Photovoltaic applications. The high absorption cross-section of colloidal QDs (cQDs) at tunable wavelengths makes them attractive for thin film solar cells, since this characteristic allows for optimal harvesting of the solar spectrum, thereby opening a promising route to high efficiency [36, 38–41]. Moreover, just like for cQD-LEDs, solution processability is a great asset, offering the prospect of low fabrication costs and easy upscaling. The exciton dissociation in cQDs is also relatively easy and can be boosted by using HNC architectures. These properties have led to the utilization of cQDs in a variety of different solar cell concepts [38, 40, 41]. The present record efficiencies, however, are still below 6 %, mostly due to low charge carrier mobility through the cQD-film and contact losses. cQDs have also been used as sensitizers in Gratzel-type solar cells (cQD sensitized solar cell, cQD-SSC), leading to 5–6 % power conversion efficiency [39]. This value is significantly lower than that achieved by dye sensitized solar cells (viz., 12 %). The losses in cQD-SSCs are mostly due to inefficient interfacial electron transfer processes and parasitic processes such as photocorrosion of the cQD [39]. cQDs can also be used as luminophores in luminescent solar concentrators (LSCs). These devices consist of a plastic plate containing a luminophore (QD or dye) that absorbs the sun light and reemits the energy at longer wavelengths. The emitted light is trapped by total internal reflection in the plate and waveguided towards the narrow facets of the LSC plate where a solar cell is mounted. The efficiency of these devices is as yet rather low, due to several loss mechanisms, of which reabsorption of the emitted light by the fluorophore itself is of high importance. The use of Type-II HNCs as luminophores in LSCs has been recently shown to greatly minimize reabsorption losses [42]. At present, there is a worldwide research effort addressing the loss mechanisms in cQD solar cells, cQD-SSCs and cQD-LSCs. It may therefore be expected that in time cQD-based solar cells will fulfil their promise of providing abundant and cheap energy.

Photocatalysis. Solar energy conversion with colloidal NSs can also be achieved through photocatalysis. In this case, the photogenerated charge carriers are used to promote redox chemical reactions, such as Hydrogen generation from water or synthesis of methanol from water and CO_2 [43]. Colloidal anisotropic Type-II heteronanocrystals in which two semiconductors and a metal are combined (e.g., ZnSe/CdS dot core/rod shell heteronanorods coupled to a Pt NC tip) have been shown to be particularly efficient in the photocatalytic generation of Hydrogen, since very fast charge separation occurs in these systems [44]. Nevertheless, the development of these systems into commercially viable photocatalystsis still hampered by an incomplete understanding of the complex chain of coupled processes that takes place between light absorption by the semiconductor and the actual splitting or formation of chemical bonds. Moreover, strategies to hinder parasitic processes (e.g., photocorrosion) must still be developed.

2.10 Outlook

This chapter has summarized the current understanding of quantum confinement effects and nanoscale excitons in semiconductor nanostructures, with particular emphasis on quantum dots. We limited ourselves to the fundamental concepts. For a more detailed and comprehensive analysis, the reader is referred to the literature. There are still some aspects that are currently not fully understood, and are the subject of on-going research. For instance, a comprehensive understanding of the exciton-phonon coupling in semiconductor nanostructures has yet to emerge. The relaxation dynamics of spatially confined excitons is also the subject of extensive investigation. Another interesting aspect that is attracting increasing attention in recent years is the investigation of colloidal semiconductor hetero-nanocrystals, which allow for a remarkable degree of control over the properties of nanoscale excitons. Electronic coupling and transport phenomena in quantum dot superlattices is also currently under intense scrutiny. These worldwide research efforts will undoubtedly deepen our understanding and provide a wealth of new insights that will pave the way to a number of as yet unforeseen applications.

2.11 Exercises

1. The absorption and emission spectra of CdTe nanocrystals ranging in diameter from 2.9 to 14.8 nm are presented in Fig. 2.23. CdTe is a direct band gap semiconductor material with a bulk band gap of 1.56 eV and an exciton Bohr radius of 7.3 nm.
   (a) How do you explain the size dependent spectral shift observed in the optical spectra?
   (b) Explain the spectral changes observed in the absorption spectra of the nanocrystals as their size is reduced.
   (c) What emission wavelength do you expect for CdTe nanocrystals with 3.7 nm in diameter?
   (d) How large is the band gap of a 30 nm diameter CdTe nanocrystal?
   (e) Do you expect that optical spectroscopy would remain an useful technique to follow the growth of CdTe nanocrystals in the 20–40 nm diameter range? Justify your answer.
2. When a quartz (SiO_2) crystal is pulverized to 5 μm particles a white powder is obtained. Do you expect any colour change if the particle size is further decreased to 10 nm? Do you expect any size effect on the properties of 10 nm SiO_2 nanocrystals? (i.e. would they differ in any way from those of the micrometer sized particles shown below?). The band-gap of SiO_2 is 7 eV (exciton Bohr radius 0.5 nm).

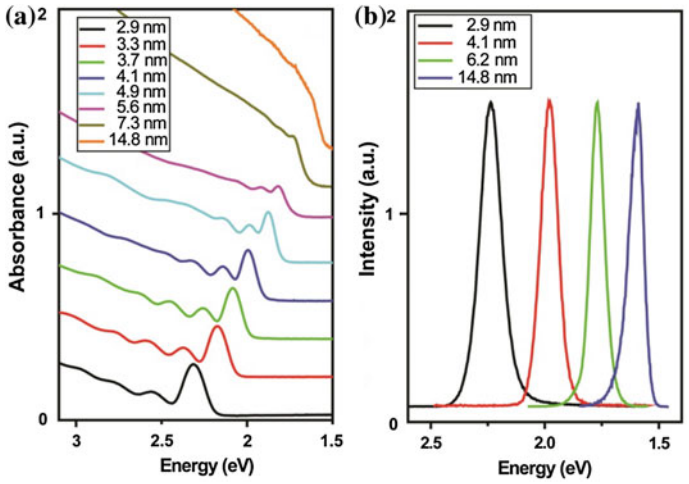

Fig. 2.23 Absorption and photoluminescence spectra of colloidal CdTe nanocrystals

3. The abstract of a paper published in a well-known scientific journal is reproduced below:
   Abstract: *Pronounced structure in X-ray excited luminescence* (*XEL*) *has been observed in dilute Tb-doped* Y_2O_3 (Y_2O_3*:Tb*) *nanocrystals. This effect affords a means to assess different energy transfer mechanisms in the nanocrystals and also an opportunity for novel device applications. Sharp jumps and oscillations are found in the XEL output with the incident X-ray energy around the absorption edges of Y and Tb. When compared with a bulk* Y_2O_3*:Tb sample, these effects are attributed to some unique electronic and optical properties of doped nanocrystals related to quantum confinement of charge carriers, and the main features can be explained by a proposed model of multichannel energy transfer. Extended X-ray absorption fine structure techniques have also been employed to study the effect of size variation and chemical doping on the local structures in* Y_2O_3 *and* Y_2O_3*:Tb nanocrystals. The local environment surrounding Y and Tb in the nanocrystals is compared with that in the respective bulk material. The results indicate that Tb impurity atoms substitute for Y sites in bulk* Y_2O_3*, while doping in the nanocrystals is complicated by the large fraction of surface atoms and local disorder.* (*C*) *1998 American Institute of Physics.*

Basically, the authors state that they observed a new phenomenon in Y_2O_3:Tb nanocrystals (viz. "*pronounced structure in x-ray excited luminescence*") and explain it by quantum confinement effects (see underlined section above).

The nanocrystals investigated range from 2.5 to 5.5 nm in diameter. The bulk band-gap of Y_2O_3 is 5.5 eV (exciton Bohr radius: 0.6 nm). Do you agree or disagree with the authors? Justify your answer.

References

1. Brynjolfsson, E., McAfee, A.: Winning the race with ever-smarter machines. MIT Sloan Manage. Rev. **53**, 53 (2012)
2. Donega, C.D.M.: Synthesis and properties of colloidal heteronanocrystals. Chem. Soc. Rev. **40**, 1512–1546 (2011)
3. Alivisatos, A.P.: Perspectives on the physical chemistry of semiconductor nanocrystals. J. Phys. Chem. **100**, 13226–13239 (1996)
4. Rossetti, R., Brus, L.: Electron-hole recombination emission as a probe of surface-chemistry in aqueous CdS colloids. J. Phys. Chem. **86**, 4470–4472 (1982)
5. Gaponenko, S.V.: Introduction to Nanophotonics. Cambridge University Press, Cambridge (2010)
6. Klimov, V.I.: Spectral and dynamical properties of multiexcitons in semiconductor nanocrystals. Annu. Rev. Phys. Chem. **58**, 635–673 (2007)
7. Efros, A.L., Rosen, M.: The electronic structure of semiconductor nanocrystals. Annu. Rev. Mater. Sci. **30**, 475–521 (2000)
8. Lo, S.S., Mirkovic, T., Chuang, C., Burda, C., Scholes, G.D.: Emergent properties resulting from Type-II band alignment in semiconductor nanoheterostructures. Adv. Mater. **23**, 180–197 (2011)
9. Kambhampati, P.: Hot exciton relaxation dynamics in semiconductor quantum dots: radiationless transitions on the nanoscale. J. Phys. Chem. C **115**, 22089–22109 (2011)
10. Henderson, B., Imbusch, G.F.: Optical Spectroscopy of Inorganic Solids. Clarendon Press, Oxford (1989)
11. Bhattacharya, P., Ghosh, S., Stiff-Roberts, A.D.: Quantum dot opto-electronic devices. Annu. Rev. Mater. Res. **34**, 1–40 (2004)
12. Elzerman, J.M., Hanson, R., van Beveren, L.H.W., Witkamp, B., Vandersypen, L.M.K., Kouwenhoven, L.P.: Single-shot read-out of an individual electron spin in a quantum dot. Nature **430**, 431–435 (2004)
13. Tian, B., Kempa, T.J., Lieber, C.M.: Single nanowire photovoltaics. Chem. Soc. Rev. **38**, 16–24 (2009)
14. Hochbaun, A.I., Yang, P.: Semiconductor nanowires for energy conversion. Chem. Rev. **110**, 527–546 (2010)
15. Hocevar, M., Immink, G., Verheijen, M., Akopian, N., Zwiller, V., Kouwenhoven, L., Bakkers, E.: Growth and optical properties of axial hybrid III-V/silicon nanowires. Nature Commun. **3**, 1266 (2012)
16. Bawendi, M.G., Steigerwald, M.L., Brus, L.E.: The quantum-mechanics of larger semiconductor clusters (quantum dots). Annu. Rev. Phys. Chem. **41**, 477–496 (1990)
17. Delerue, C., Lannoo, M.: Nanostructures: Theory and Modelling. Springer, Berlin (2004)
18. An, J.M., Franceschetti, A., Dudiy, S.V., Zunger, A.: The peculiar electronic structure of PbSe quantum dots. Nano Lett. **6**, 2728–2735 (2006)
19. Koole, R.: Fundamentals and applications of semiconductor nanocrystals Ph.D. Thesis, Utrecht University, Utrecht (2008)
20. Wright, J.C.: Chemistry 623 Notes-Experimental Spectroscopy. Dept. of Chemistry, University of Wisconsin, pp. 47–69 (1990)
21. Lodahl, P., van Driel, A.F., Nikolaev, I.S., Irman, A., Overgaag, K., Vanmaekelbergh, D., Vos, W.L.: Controlling the dynamics of spontaneous emission from quantum dots by photonic crystals. Nature **430**, 654–657 (2004)
22. Rogach, A.L., Klar, T.A., Lupton, J.M., Meijerink, A., Feldmann, J.: Energy transfer with semiconductor nanocrystals. J. Mater. Chem. **19**, 1208–1221 (2009)
23. Förster, T.: Energiewanderung und Fluoreszenz. Naturwissenshaften **33**, 166–175 (1946)
24. Reiss, P., Protière, M., Li, L.: Core/shell semiconductor nanocrystals. Small **5**, 154–168 (2009)
25. Pandey, A., Guyot-Sionnest, P.: Intraband spectroscopy and band offsets of colloidal II-VI core/shell structures. J. Chem. Phys. **127**, 104710 (2007)

26. Ivanov, S.A., Piryatinski, A., Nanda, J., Tretiak, S., Zavadil, K.R., Wallace, W.O., Werder, D., Klimov, V.I.: Type-II core/shell CdS/ZnSe nanocrystals: Synthesis, electronic structures, and spectroscopic properties. J. Am. Chem. Soc. **129**, 11708–11719 (2007)
27. Donegá, C.D.M.: Formation of nanoscale spatially indirect excitons: evolution of the type-II optical character of CdTe/CdSe heteronanocrystals. Phys. Rev. B **81**, 165303 (2010)
28. Grodzińska, D., Evers, W.H., Dorland, R., van Rijssel, J., van Huis, M.A., Meijerink, A., de Mello Donegá, C., Vanmaekelbergh, D.: Two-Fold emission from the S-Shell of PbSe/CdSe core/shell quantum dots. Small **7**, 3493–3501 (2011)
29. Klimov, V.I., Ivanov, S.A., Nanda, J., Achermann, M., Bezel, I., McGuire, J.A., Piryatinski, A.: Single-exciton optical gain in semiconductor nanocrystals. Nature **447**, 441–446 (2007)
30. Pandey, A., Guyot-Sionnest, P.: Slow electron cooling in colloidal quantum dots. Science **322**, 929–932 (2008)
31. He, J., Lo, S.S., Kim, J., Scholes, G.D.: Control of exciton spin relaxation by electron-hole decoupling in type-II nanocrystal heterostructures. Nano Lett. **8**, 4007–4013 (2008)
32. Kim, S., Fisher, B., Eisler, H., Bawendi, M.: Type-II quantum dots: CdTe/CdSe(core/shell) and CdSe/ZnTe(core/shell) heterostructures. J. Am. Chem. Soc. **125**, 11466–11467 (2003)
33. Shirasaki, Y., Supran, G.J., Bawendi, M.G., Bulovic, V.: Emergence of colloidal quantum-dot light-emitting technologies. Nat. Photon. **7**, 13–23 (2013)
34. Bimberg, D., Pohl, U.W.: Quantum dots: promises and accomplishments. Mater. Today **14**, 388–397 (2011)
35. Garcıa-Santamarıa, F., Chen, Y., Vela, J., Schaller, R.D., Hollingsworth, J.A., Klimov, V.I.: Suppressed Auger recombination in "giant" nanocrystals boosts optical gain performance. Nano Lett. **9**, 3482–3488 (2009)
36. Konstantatos, G., Sargent, E.H.: Colloidal quantum dot optoelectronics and photovoltaics. Cambridge University Press, Cambridge (2013)
37. Doane, T.L., Burda, C.: The unique role of nanoparticles in nanomedicine: Imaging, drug delivery and therapy. Chem. Soc. Rev. **41**, 2885–2911 (2012)
38. Lunt, R.R., Osedach, T.P., Brown, P.R., Rowehl, J.A., Bulovic, V.: Practical roadmap and limits to nanostructured photovoltaics. Adv. Mater. **23**, 5712–5727 (2011)
39. Kamat, P.V.: Boosting the efficiency of quantum dot sensitized solar cells through modulation of interfacial charge transfer. Acc. Chem. Res. **45**, 1906–1915 (2012)
40. Kramer, I.J., Sargent, E.H.: Colloidal quantum dot photovoltaics: a path forward. ACS Nano **5**, 8506–8514 (2011)
41. Nozik, A.J., Conibeer, G., Beard, M.C.: Advanced concepts in photovoltaics. Royal Society of Chemistry, Oxford (2014)
42. Krumer, Z., Pera, S.J., van Dijk-Moes, R.J.A., Zhao, Y., de Brouwer, A.F.P., Groeneveld, E., van Sark, W.G.J.H.M., Schropp, R. E.I., Donega, C.D.M.: Tackling self-absorption in luminescent solar concentrators with type-II colloidal quantum dots. Sol. Energy Mater. Sol. Cells **111**, 57–65 (2013)
43. Fan, W., Zhang, Q., Wang, Y.: Semiconductor-based nanocomposites for photocatalytic H_2 production and CO_2 conversion. Phys. Chem. Chem. Phys. **15**, 2632–2649 (2013)
44. O'Connor, T., Panov, M.S., Mereshchenko, A., Tarnovsky, A.N., Lorek, R., Perera, D., Diederich, G., Lambright, S., Moroz, P., Zamkov, M.: The effect of the charge-separating interface on exciton dynamics in photocatalytic colloidal heteronanocrystals. ACS Nano **6**, 8156–8165 (2012)
45. Groeneveld, E.: Synthesis and optical spectroscopy of (hetero)-nanocrystals. Ph.D. Thesis, Utrecht University, Utrecht (2012)
46. Koole, R., Allan, G., Delerue, C., Meijerink, A., Vanmaekelbergh, D., Houtepen, A.J.: Optical Investigation of Quantum Confinement in PbSe Nanocrystals at Different Points in the Brillouin Zone. Small **4**, 127–133 (2008)
47. Link, S., El-Sayed, M.A.: Size and temperature dependence of the plasmon absorption of colloidal gold nanoparticles. J. Phys. Chem. B **103**, 4212–4217 (1999)

http://www.springer.com/978-3-662-44822-9

Nanoparticles
Workhorses of Nanoscience
de Mello Donega, C. (Ed.)
2014, XII, 299 p. 140 illus., 53 illus. in color., Hardcover
ISBN: 978-3-662-44822-9